Automated Feature Extraction of Shear Layers in CFD Simulations

by

Lawrence Jared Baskett

B.S. Mechanical Engineering
Stanford University, 1999

Submitted to the Department of Aeronautics and Astronautics
in partial fulfillment of the requirements for the degree of

Master of Science in Aeronautics and Astronautics

at the

MASSACHUSETTS INSTITUTE OF TECHNOLOGY

February 2002

Author .....
Department of Aeronautics and Astronautics
February 1, 2002

Certified by .....
Robert Haimes
Principal Research Engineer
Thesis Supervisor

Accepted by .....
Wallace E. Vander Velde
Professor of Aeronautics and Astronautics
Chair, Committee on Graduate Students

Automated Feature Extraction of Shear Layers in CFD Simulations

by

Lawrence Jared Baskett

Submitted to the Department of Aeronautics and Astronautics
on February 1, 2002, in partial fulfillment of the
requirements for the degree of
Master of Science in Aeronautics and Astronautics

Abstract

This thesis demonstrates a generalized method for extracting shear layers as features in viscous computational fluid dynamics flowfields. A source term indicative of shear in the flow combines with convective terms to constitute a conservation equation for a scalar shear layer detector variable. The source terms explored in this investigation come from the viscous terms of the Navier-Stokes momentum equations as well as from a simple shear measure obtained from the velocity gradient tensor. A threshold value of the scalar detector variable indicates the boundary layer or wake edge, while the magnitude of the detector indicates the intensity of shear influence upon any particular point in the flow. Test cases validate the convective technique and demonstrate its rejection of false sources. Among the applications of shear layer feature extraction are solution improvement techniques like grid adaptation and tools for analysis and design such as visualization.

Thesis Supervisor: Robert Haimes
Title: Principal Research Engineer

Acknowledgments

Finding myself at the end of over two years of effort, it is humbling to look back at how much I have discovered about the nature of learning, motivation, friendship, and the formation of ideas, in addition to computational fluid dynamics. I would like to extend my sincere gratitude to Bob Haimes for the great opportunity to do this work with him and for his honesty and patience. I am very grateful to David Kenwright for also serving as my advisor during his brief but eventful stay here.

Many thanks to Prof. Mark Drela for his theoretical insights and for his assistance with MSES modifications. Of the students of the Fluid Dynamics Research Laboratory, I am most indebted to David Venditti. He provided assistance in a multitude of ways: grid generators and datasets as well as feedback, encouragement, and friendship. Thanks also to Ali Merchant for the Euler solver that served as the initial framework for my code and to Tolulope Okusanya for his Cplot plotting program. To all of the students in the lab, it would have been a much tougher ride without you there. Thanks to Adam, Ricardo, Tony, and Joe for putting up with my music and rantings and for sharing our little corner of MIT.

I have been extremely lucky to have the boundless support of my family and friends. Andrea and Jonathan, you stood by me through the highs and lows and still told me I could make it. Matt, Jon, Rob, and Yee, thanks for seeing me through it all. Finally, I owe my deepest thanks to my parents and sister for their great and unwavering love, help, and understanding.

This work was partially sponsored by NAS at NASA Ames Research Center with David Kao as the Technical Monitor and by Army Research Labs with Stephen Davis as the Technical Monitor.

Contents

1 Introduction **13**

1.1 Feature Extraction 14

1.2 Shear Layers 19

1.2.1 Scope and Significance 19

1.2.2 Definition 20

1.2.3 Alternative Definitions: Integrated Thicknesses 22

1.3 Synthesis: Shear Layer Feature Extraction 24

1.3.1 Goals and Challenges 24

1.3.2 Applications and Utilities 25

2 Theory and Approach **27**

2.1 Shear Detection Methods 27

2.1.1 Line Integration 28

2.1.2 Scalar Iso-Surface 28

2.1.3 Prior Work 34

2.2 Shear Detector Formulations 36

2.2.1 Navier-Stokes Equations Viscous Terms Source 36

2.2.2 Velocity Gradient Tensor Quantities Source 37

2.2.3 Hypothesized Applicability 38

3 Two-Dimensional Implementation and Verification **39**

3.1 Implementation 39

3.1.1 Flow Solver 39

3.1.2 Mesh 41
3.1.3 Visualization 42
3.2 Test Cases 42
3.2.1 Flat Plate 42
3.2.2 NACA 0005 Airfoil 52
3.2.3 Transonic RAE 2822 Airfoil 60
3.2.4 Multielement Airfoil 61

4 Three-Dimensional Approach **67**
4.1 Shear Detector Formulations 67
4.1.1 Navier-Stokes Equations Viscous Terms Source 68
4.1.2 Velocity Gradient Tensor Quantities Source 68
4.2 Verification 74

5 Conclusions **75**
5.1 Validity and Generality 75
5.2 Further Development 77

Bibliography **79**

List of Figures

1-1 Vortex feature visualization using dye 16

1-2 Vortex feature visualization using smoke 16

1-3 Vortex feature visualization using Doppler velocimetry 16

1-4 Vortex core feature extraction 18

2-1 Elemental deformation decomposition 30

2-2 Elemental simple shear decomposition 31

3-1 Flat plate grid 45

3-2 Flat plate velocity field 45

3-3 Flat plate x-velocity contours 46

3-4 Flat plate y-velocity contours 46

3-5 Flat plate Mach number contours 47

3-6 Flat plate source term contours 47

3-7 Flat plate shear detector contours 47

3-8 Flat plate shear detector contours, $Re = 5 \times 10^3$ 48

3-9 Flat plate velocity profile dissipation dependence 48

3-10 Flat plate velocity profile 49

3-11 Flat plate source term profile 49

3-12 Flat plate shear detector profile 50

3-13 Flat plate shear detector contours, $M = 0.7$ 51

3-14 Flat plate shear detector Mach dependence 51

3-15 Flat plate VGT source term contours 52

3-16 Flat plate VGT shear detector contours 52

3-17 Flat plate VGT source term profile 53
3-18 Flat plate VGT shear detector profile 53
3-19 Flat plate VGT shear detector Mach dependence 54
3-20 NACA 0005 original grid 55
3-21 NACA 0005 refined grid 55
3-22 NACA 0005 original grid detail 56
3-23 NACA 0005 refined grid detail 56
3-24 NACA 0005 original grid Mach contours 56
3-25 NACA 0005 refined grid Mach contours 57
3-26 NACA 0005 MSES Mach contours 57
3-27 NACA 0005 shear detector contours 57
3-28 NACA 0005 shear detector contour detail 58
3-29 NACA 0005 shear detector contour detail, $Re = 1 \times 10^5$ 58
3-30 NACA 0005 shear detector contour detail, $M = 0.2$ 58
3-31 NACA 0005 visualization 59
3-32 NACA 0005 visualization, $Re = 1 \times 10^5$ 59
3-33 RAE 2822 grid 61
3-34 RAE 2822 Mach contours 61
3-35 RAE 2822 MSES Mach contours 62
3-36 RAE 2822 shear detector contours 62
3-37 RAE 2822 entropy contours 62
3-38 RAE 2822 Mach contour detail 63
3-39 RAE 2822 shear detector contour detail 63
3-40 RAE 2822 VGT shear detector contour detail 63
3-41 RAE 2822 turbulent viscosity contours 64
3-42 RAE 2822 turbulent viscosity contour detail 64
3-43 Three element airfoil visualization 65

List of Tables

3.1 Shear detector threshold Reynolds number dependence 44
3.2 Shear detector threshold Reynolds number dependence, scaled grid . 44

Chapter 1

Introduction

An ideal put forth in the computational fluid dynamics (CFD) community is that of the "virtual wind tunnel."[1] If computation gains the ability to fully reproduce the fluid flow in a physical wind tunnel, namely real-time unsteady three-dimensional flow modeling that allows the investigator to measure and visualize the flow's character, the result will be even better than a physical wind tunnel. In that idealized case a CFD suite could model a test object in full scale, distortion-producing struts and measuring instruments and even the wind tunnel itself deleted, geometry readily modified, and the influence of such effects as jet engine intake and exhaust incorporated. The perfect CFD package would simulate, in the example of an aircraft, all flight regimes realistically and present the results in both numerical and physically intuitive visual terms. Such a package could enable the design optimization of an aircraft across the entire flight envelope.

Although computational capacity is the most obvious obstacle to progress in achieving the flow modeling fidelity necessary for a virtual wind tunnel, sophisticated and clever algorithms and techniques can reduce the level of capacity required. Methods that both encompass very generalized applicability as well as produce targeted, meaningful results make CFD more efficient and broaden its reach, even if a complete virtual wind tunnel suite is not attainable in the near future. It is hoped

[1] In fact, a NASA Ames project carries this name.

that the material presented in this thesis will constitute a small element in the family of computational tools that eventually make practical a virtual wind tunnel.

1.1 Feature Extraction

One essential element of the virtual wind tunnel ideal is feature extraction, which within a given flow involves the identification of regions that exhibit a particular behavior. Flow features within a volume of fluid include shock surfaces, vortex cores, recirculation zones, and shear layers. Fluid flow features on solid surfaces include attachment and separation lines, stagnation points being a subset of these. The state of the art in feature extraction addresses all of these features with success varying from rudimentary or situation-specific to widely applicable [13] [17]. The one exception is shear layers, which remain to be adequately isolated. Such is the task attempted in this thesis.

In this investigation, for which a physics-based perspective is emphasized over a raw mathematical one, it is instructive to take a step back and examine what constitutes feature extraction in real physical flows. The frequent emphasis on imagery often places physical feature identification techniques into the category of visualization rather than feature extraction, i.e. the investigator infers features from visual information. Feature identification in an environment such as a wind tunnel or a water channel is a process requiring much care and skill, to such a degree that some consider it as much art as science. The span of physical feature identification techniques encompasses flow markers such as smoke and dye, lighting configurations such as sheets of light that illuminate planes within the flow, photographic methods such as stroboscopy and Schlieren photography, direct sampling of flow properties with probes, and a host of other schemes.

Beyond taking care not to excessively distort the flow feature of interest, the investigator must either possess accurate foreknowledge of the feature's location and extent or else conduct a thorough search of the entire flowfield, lest any feature go unfound. The whole process is often expensive in terms of the experience, time,

and resources required, and the physical apparatus is usually difficult to modify. Often, time and physical constraints limit the number of measurements taken. Once characterized, however, flow features can reveal physical mechanisms that influence the flowfield locally and sometimes globally. High-definition images of flow features often appear so intriguing and even beautiful that books are devoted to them [25].

For example, the F/A-18 aircraft directly benefitted from feature identification work. It was discovered that, when the aircraft flies at high angles of attack, the vortex trailing from each wing leading edge extension breaks down, or "bursts," in the vicinity of the vertical tail. The vortices, if left to themselves, cause fatigue in the tails and reduce their service life. Figure 1-1 shows a dye-in-water visualization on a model that indicated the proper smoke release points for the flight test in Figure 1-2. Notice also the tufts on the wing of the flight test aircraft that give hints about the flowfield surrounding the vortices. In Figure 1-3, Doppler laser velocimetry quantifies the entire vortex flowfield. These tests illustrate the problem successfully, albeit at much expense.

Feature extraction techniques for CFD traditionally follow the lead of physical methods both in terms of configuration and the requirement for human manipulation. Manual or interactive techniques for simulated flows include locating iso-surfaces of flow properties, taking cutting planes through the solution to produce planar contour plots, using streamlines to probe the velocity vector field, and examining the velocity field directly.

In CFD, assuming the presence of a valid flow solution, the complete state of the flow is available at every node in the domain. Interpolation makes the nodal state constitute a continuum state across the domain. A complete replication of a physical flow can involve a huge quantity of data if the simulation represents complicated geometries in three dimensions with unsteady effects. Until the past decade or two only simple models, such as two-dimensional steady simulations on relatively small grids, were practical for general engineering use. The small amount of data present allowed human investigators to draw conclusions about the behavior of the flow via manual observation of the modeled flow solution. Manual methods worked reasonably well,

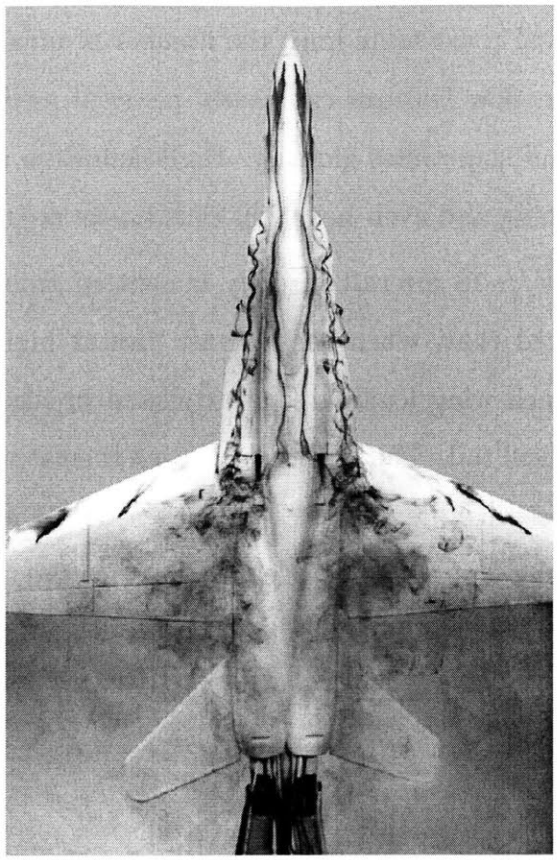

Figure 1-1: Experimental feature identification: F/A-18 model leading edge extension vortex visualization using dye in a water channel [9]

Figure 1-2: Experimental feature identification: F/A-18 leading edge extension vortex visualization using smoke in flight [9]

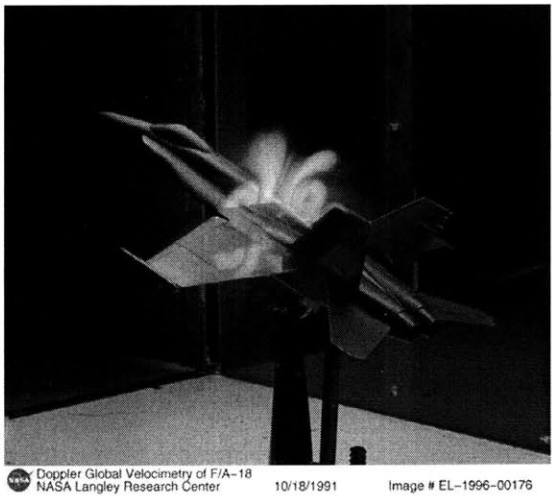

Figure 1-3: Experimental feature identification: F/A-18 model leading edge extension vortex measurement using Doppler laser velocimetry [18]

although they have many of the same drawbacks of physical feature identification, namely they require time investment on the part of the investigator, some practice, and usually partial foreknowledge of the flow topology.

In a 3-D simulation or even a 2-D simulation with substantial flow complexity, these methods grow to be rather cumbersome in their demands upon the investigator. In many time-varying simulations, manual techniques as a practical matter break down completely due to the need for attention to every time step. They have further disadvantages comparable their physical counterparts: a thorough search the flowfield dataset is often impractical; frequently the flow around and through the feature is illustrated but not the feature itself; and after only a few "visualization objects" like iso-surfaces or streamline ribbons are put in place, the overabundance of images on the display obscures the features that the investigator was trying to find in the first place [11].

Automated data reduction is crucial to the thorough analysis of realistically modeled complex fluid flows. Beyond avoiding the aforementioned disadvantages of interactive methods, automatic feature extraction opens up a range of computational benefits to CFD simulations. As pointed out by Haimes [11], automation allows a CFD suite to run a separate feature extraction batch computation and to apply the results toward solution improvement in the course of a simulation. Note that beyond post-processing a pre-converged solution, batch computation raises the possibility of feature extraction's use in a co-processing sense as the solution progresses. Vehicles for solution improvement include refining feature resolution through grid adaptation, which is one of the most practical of all applications of feature extraction, as well as boundary condition modification where fluid features intersect the edge of the domain. When the extraction technique is local in space and time, it lends itself readily to parallelization. When the feature extraction results constitute the output data in the place of the flow complete solution, the reduction in dataset size is typically several orders of magnitude. Data reduction relaxes the demanding storage space requirement for large simulations and facilitates visualization, particularly for animations of unsteady solutions. Feature extraction can also make available quantitative infor-

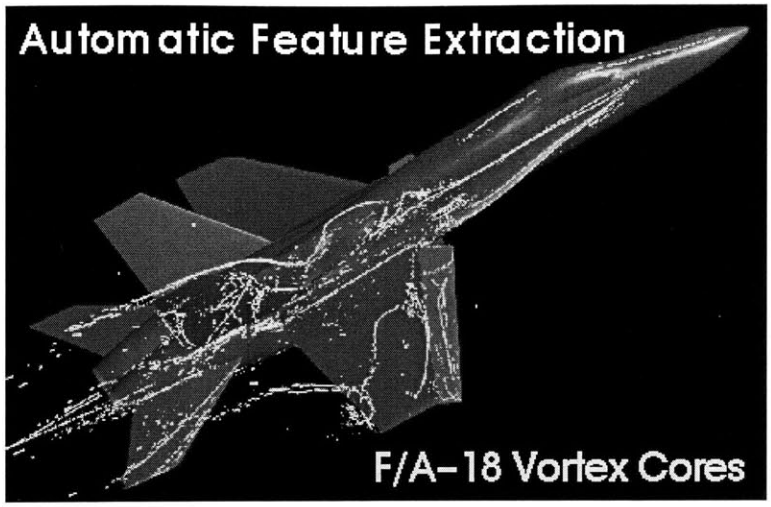

Figure 1-4: Feature extraction of the vortex cores on an F/A-18 using FX [15]

mation such as the exact location and in some cases the strength of the features in question. Feature extraction can drive a targeted calculation to find, for example, the severity of a shock or an integrated characteristic of a boundary layer cross-section.

Pre-convergence feature information, when visualized by the investigator, can indicate how well the computational run is progressing. The investigator could then decide whether to scrap the run or to adjust the numerical conditions or geometry as iterations progress, a process known as solution steering. Visualization in general is a feature extraction application in its own right. Beyond its use for solution steering, visualization converts the solution from a field of numbers to a physical representation that humans can more readily digest. Feature extraction-driven visualization directly illuminates the structure of the most critical and relevant portions of a flowfield, bypassing the aforementioned difficulties that hinder manual techniques. Figure 1-4 demonstrates how, so long as the flow solution is accurate, feature extraction effectively elucidates the flow structure. The vortex core above the leading edge extension is the same as the cores visualized in Figures 1-1 through 1-3. Note the fence added at the wing root leading edge that causes the leading edge extension vortex to burst over the wing, preventing tail fatigue.

The information provided by feature extraction can be applied toward visual-

ization, improvement of the solution, and quantitative analysis of the features in question. Feature extraction neither passes on the entire state of the flow nor reduces the state to a single performance parameter. It instead takes the intermediate path of elucidating the structure of the flow by isolating the most significant flow regions and categorizing them. Feature extraction bridges the gap between computational fluid flow modeling and presentation or visualization of the model in a way that humans can easily absorb. From a design perspective, the seamless integration of this line of computational analysis will allow capabilities beyond raw performance analysis of an aircraft, such as finding the lift-to-drag ratio at several design points. Feature extraction engenders the ability to qualitatively and quantitatively consider the topology of the flow when optimizing aircraft performance, either at a particular flight condition or across a range of conditions. Once knowledge of a flow's structure is obtained automatically, through an analysis suite the investigator can explore where losses occur and how strong they are in a flow and then alter the geometry to improve relevant performance characteristics. This investigation aims to contribute a small bit of the computational chain that makes the ideal of a virtual wind tunnel a practicality.

1.2 Shear Layers

1.2.1 Scope and Significance

For the purposes of this investigation, the scope of flow features covered by the term "shear layers" includes laminar and turbulent boundary layers, wakes, and regions of free shearing flow such as the mixing layer between a jet of fluid and the ambient fluid surrounding it. Shear layers are highly significant for fluid mechanical engineering applications because they are the manifestation of viscous effects, notably loss mechanisms like surface friction, flow blockage, and separation. They also influence the flow downstream in the form of a wake and constitute the interaction between zones of differing flow velocity in the case of a free shear layer.

Shear layers are regions where large gradients of velocity and other flow properties

are present, where vorticity generation takes place, and where turbulence can occur. For shear layers to be distinguishable within a flowfield, inertial forces must dominate over viscous forces for the bulk of the flow; i.e. the Reynolds number must be much greater than unity [27]. Note that a vortex core originates in a boundary layer and is encompassed in the resulting wake, so it falls under the shear layer umbrella. Separated flow too is a subset of shear layers, as are recirculation regions. In fully developed internal flows, shear layers have merged to cover the entire flowfield, so special consideration may be necessary for such flows.

1.2.2 Definition

Defining the extent of a shear layer is difficult and in a sense arbitrary. The definition is clearest in the case of fully attached, incompressible, laminar boundary layer flow along a stationary flat plate. If while moving out normal from the wall one measures the flow velocity parallel to the wall, one finds that it varies smoothly from zero right at the wall out to a "freestream" velocity characteristic of the bulk of the flow. The freestream is uniform in the Blasius definition [10] or governed by inviscid forces (though influenced by the presence of shear layers) in general. Although, strictly speaking, the boundary layer's edge should be located where the flow velocity reaches the freestream value, in theory the velocity profile approaches that value asymptotically. δ denotes the distance from the solid surface to the boundary layer edge. The edge of the boundary layer or of a shear layer in general is most broadly the point at which the effects of viscous shear become insignificant.

How significant is insignificant? Let us return to the flat plate example. There is no critical surface or distinct property that marks the boundary layer edge. Any edge definition contains some degree of arbitrariness due to the asymptotic variation of the velocity profile, but some absolute definition must be set, lest we entirely give up on locating shear layers! We take the edge of the boundary layer to be the point in the profile at which the velocity reaches a set percentage of the freestream value. Any cutoff value, such as 95% of the freestream velocity relative to the wall, could be valid. Here we choose the boundary layer edge to be located where the flow

reaches 99% of the freestream velocity, or a distance from the wall of δ_{99}, such that the definition includes as much of the boundary layer as possible while ignoring any minor fluctuations in the velocity field. δ_{99} sees frequent use in engineering practice.

Implicit in the above discussion is the knowledge of the edge velocity u_{edge}, which for any case other than the Blasius flat plate example is not necessarily a uniform freestream value. Given a flowfield, finding the edge velocity assumes that one knows where the boundary layer edge is, which brings us back to the goal of the shear layer feature extraction technique that this thesis attempts to address.

Although in simple viscous flows one thinks of the edge of the boundary layer as located where the flow velocity parallel to the surface attains or almost attains freestream velocity, the most general shear layer definition would ignore such geometry considerations. In some cases, such as attached flow over a flat plate, over a two-dimensional airfoil, or in a two-dimensional duct, the numerical value of the boundary layer thickness can be found (see the following discussion on interacting boundary layer theory). In other cases including massively separated flow, the association of a quantitative value with the distance from a solid surface to the shear layer edge begins to lose relevance since the flow velocity at the edge may not be at all parallel to the surface in question. In the case of a wake, there is no surface to reference at all, and for asymmetric or irregular wake velocity profiles, any definition of a reference centerline will be arbitrary. In the case of three-dimensional boundary layers, flow can change direction through the velocity profile such that the velocity component perpendicular to the freestream flow direction is nonzero. One could establish different boundary layer thicknesses for a single surface point based upon velocity profiles in two orthogonal directions.

In order to ensure complete generality, a single all-encompassing 3-D shear layer thickness definition is desired. Although this discussion describes δ_{99} for simple flow geometries and gives a sense of what a fully general definition of δ might entail, no such definition statement is currently available or perhaps even possible. This thesis hypothesizes that a shear layer feature extraction technique that matches a given δ for all available test cases will be applicable to any viscous flow.

Interacting Boundary Layer Theory

Flow solvers that use interacting boundary layer theory (IBLT) directly solve for boundary layer properties, such as the edge location and velocity. These solvers, one example of which is MSES [7], model the boundary layer and the surrounding inviscid flow as distinct zones. They match flow conditions between the two via the boundary layer displacement thickness (see Section 1.2.3) and the state of the flow where the zones meet. Because IBLT models require no shear layer feature extraction thanks to the boundary layer representation already contained within the solver, such models provide useful reference cases for feature extraction tools that operate on more general Navier-Stokes models. Unlike IBLT models, which at present apply primarily to two-dimensional or axially symmetric geometries with predominantly attached flow, models employing the Navier-Stokes equations represent flows under any conditions.[2]

1.2.3 Alternative Definitions: Integrated Thicknesses

An alternative means of characterizing boundary layers and wakes is to perform integrals to quantify the physical effects of their presence. Key examples include the displacement thickness δ^*, which represents how much an equivalent inviscid flow would be displaced from the surface to match the actual flow, and the momentum thickness θ, which accounts for how much flow would have to be removed from the equivalent inviscid flow to account for the momentum lost in the boundary layer. δ^* provides an indication of how the boundary layer shapes the outer flow and of how much flow blockage is present. θ is less relevant for illustrating the extent of the boundary layer but more significant when evaluating forces in the flow, namely surface friction drag.

Integrated thicknesses have precise definitions that allow exact quantitative characterization of boundary layers nominally without subjectivity, with the caveat that

[2]Of course, in the case of the Reynolds-averaged Navier-Stokes equations, we assume here that they completely represent continuum flow physics and that the turbulence model is accurate.

it must be possible to define the integration. The integration is carried out along a line normal to a solid surface, starting at the surface and ending in the potential flow just outside of the boundary layer. For simplicity, the incompressible form is stated here.

$$\delta^* = \int_0^\delta \left(1 - \frac{u}{u_{edge}}\right) \mathrm{d}y \tag{1.1}$$

$$\theta = \int_0^\delta \left(1 - \frac{u}{u_{edge}}\right) \frac{u}{u_{edge}} \mathrm{d}y \tag{1.2}$$

The integrals require knowledge of location and velocity at the edge of the boundary layer, information that as mentioned is unknown without having a feature extraction tool to find it. Another complicating issue is the need to construct an integration path normal to the solid surface everywhere that the thickness is calculated. In regions of high curvature the "normals" might not even be straight lines, particularly in concave geometries where straight normal lines would intersect each other and possibly even run into other surfaces. Wakes introduce a host of difficulties due to the lack of a reference surface. Some kind of wake centerline, which as noted before may have arbitrary placement, might be required to construct integration paths and place in space the surfaces the integrals produce.

In three dimensions the difficulties of choosing a flow direction mentioned before are compounded because the whole velocity profile must be considered, not just the edge velocity. High surface geometry curvature crosswise to the prevailing flow robs the above one-dimensional definition of its accuracy. A stopgap correction is to employ local radial coordinates [19]. Two-dimensional integration in a plane perpendicular to the flow would restore accuracy in the form of an integrated area instead of thickness, i.e. a displacement area Δ^* or momentum area Θ. Area boundary layer characterizations add yet another degree of integration complexity, however, and they absorb boundary layer data from the integral surfaces into a de-localized parameter that may only be truly meaningful in a wake.

1.3 Synthesis: Shear Layer Feature Extraction

1.3.1 Goals and Challenges

Given the significance of feature extraction and specifically extraction of shear layers, let us now detail the attributes of an ideal shear layer feature extraction tool. For any particular simulation, a shear layer feature extraction tool needs to identify the volume of fluid representative of all shear layers present in the flow, as bounded between the shear layer edge surfaces (where shearing flow meets the surrounding flow) and any solid surfaces.

A versatile shear detector functions for laminar and turbulent flows at all Mach and Reynolds numbers of engineering interest. Note that turbulent flow simulations employing a Reynolds-averaged Navier-Stokes model will exhibit smooth shear layer edges, like laminar flows, while transient large-eddy simulation (LES) and direct numerical simulation (DNS) flow representations will have irregular shear layer edges that fluctuate with time. Any finite Mach number should be acceptable, while the range of relevant Reynolds numbers is that much greater than unity [27].

The importance of computational efficiency means that the ideal detector operates on flow properties that are as local as possible. The detector should be numerically resilient, self-contained, automatic, and general to any geometry. No foreknowledge of u_{edge} should be required.

After overcoming the indistinct nature of boundary layers and wakes, the second most challenging hurdle for a shear detector is the ability to ignore regions of the flow that may exhibit properties similar to shear layers but are not in fact shear layers. Most prominent among such regions are shocks and vortices, the other most significant objects of feature extraction. Shocks can be problematic due to the strong variation in flow properties across them. Curved shocks may cause more difficulties than normal shocks because, within the former, shear can take place. As mentioned with respect to vortices, incorporating the vortex core into the volume of shear layers is actually desirable because it is part of the wake, although the surrounding swirling flow should not be included.

1.3.2 Applications and Utilities

Investigators involved in many applications of CFD would find a shear layer extraction tool highly useful. We have already discussed solution improvement through grid refinement and boundary condition modification. A universal shear layer extractor could also form the nucleus of a new turbulence model or of a laminar/turbulent transition prediction method.

Visualization brings the extracted information to the engineer in a manner useful for design. For instance, given a three-dimensional interaction of boundary layers at a jet engine nacelle/pylon junction, a visualization of the shear layer edge as a single surface indicates how the boundary layers on intersecting surfaces interact. Visualization of the wakes trailing from a blade row in a turbine engine can lead to better understanding of rotor/wake interaction. In this case the investigator could visualize the wakes of each blade row separately to see their influence even through a succession of stages. Additional pertinent applications include the assessment of helicopter rotor wake effects, the characterization of turbine engine endwall leakage flows, and many others. Knowledge of where shear layers lie allows the investigator to *know* rather than guess how surface geometry effects shear flows and their influence upon the complete flowfield.

Chapter 2

Theory and Approach

As we have seen, the primary challenge in distinguishing shear layers from the rest of a flow is that there is no definite flow property demarcation or numerical criticality that marks the shear layer edge. The next section lays out some possible means of attacking the shear layer feature extraction problem, and after that the discussion delves into the approaches adopted for full development.

2.1 Shear Detection Methods

The advantages of choosing the extreme edge of shear layers as the bound for our feature extraction tool are multifold. First of all, within the outer edge all shear effects in the flow are covered, so the remainder of the flow behaves in an effectively inviscid manner. If the edge can be found without making reference to say normals from a solid surface, then the shear detector will be able to accommodate arbitrary geometries. Alternative shear layer volume characterization techniques exist, namely integrated boundary layer thicknesses that have to do with the physical effects of shear layers upon the overall flow (see Section 1.2.3), but these are not pursued in this investigation for reasons detailed in the following discussion.

2.1.1 Line Integration

Several drawbacks of using integrated thicknesses for feature extraction are apparent. The integrals require knowledge of location and velocity at the edge of the boundary layer, information that as mentioned is unknown without having a feature extraction tool to find it or some other way of divining it. Integration thicknesses also demand the construction of integration paths, which depend upon surface geometry and perhaps flow topology. If the latter is included, the path construction contributes substantially to computational expense, particularly in unsteady simulations.

When superimposed upon the flow solution, the surfaces defined by integrated thicknesses do not contain the full range of shear influence upon the flow, although one important advantage is that they do provide useful information on the physical impact of that shear influence. In three dimensions the aforementioned difficulties of choosing a flow direction are compounded because the whole velocity profile must be considered. To perform wake calculations the software must know that a wake is present in the first place, for which a generalized shear layer extractor again might be necessary.

For simple geometries with predominantly attached flow, however, an integrated boundary layer thickness approach can be made to work as a feature extractor that demonstrates good accuracy against baseline data, as presented by Lovely [19] and summarized in the Section 2.1.3. This investigation instead attacks the more general problem of finding the outer edge of the shear layer.

2.1.2 Scalar Iso-Surface

Scalar iso-surfacing is a volume-based approach to shear layer extraction. It aims to use some scalar property that is zero or some other known constant outside of shear layers but active for the flow inside them. An iso-surface at a threshold value slightly above the freestream constant marks the divide between the two portions of the flow corresponding to the shear layer edge. The variation of the scalar property within shear layers can also serve as an indicator of the local degree of shear influence upon

the flow.

Local State Property

Were some state property within the flow to indicate the presence of a shear layer, it would provide a computationally cheap detector. The calculation of a local property from the flow solution would require nothing more than the solution state information at each particular node and perhaps also at the neighboring nodes. Of the physical state properties, entropy and stagnation enthalpy appear most promising. Topological characteristics of the velocity vector field may also provide a measurement of flow structure characteristics indicative of shear layers. As tantalizingly promising as are the results of attempted local property-based shear layer identification, ambiguities in their application introduced by sources other than shear layers render this technique impractical.

Entropy is a physical measure of the degree of viscous influence upon a fluid. It is a relative quantity, so an arbitrary reference value, typically the freestream value, must be established such that the rest of the flow is compared to it. The appeal of entropy as a shear detector stems from entropy generation in regions of high shear gradients and the subsequent convection of entropy that marks the entire shear layer. That said, shocks, vortex cores, shear layers, and regions of heat transfer all generate entropy. Even considering the relative strength of shear layer sources, at least in nearly adiabatic flows where shocks and vortices are negligible, the generation of entropy in other regions regions means that it is noisy and imprecise as an extraction tool. Stagnation enthalpy at first glance appears more appropriate because stationary shocks do not effect it, but its use as a shear layer indicator requires a Prandtl number close to unity, and it suffers some of the same difficulties as entropy [19]. Both stagnation enthalpy and entropy pick up numerical noise during the CFD solution process because they are not directly conserved [8]. One way around this particular difficulty is to set up a separate conservation equation that depends upon the solver's state vector, although such a fix would increase the computational expense of the extraction tool without removing physically fundamental inaccuracies.

Another approach recognizes that shear layers have a unique topological structure in the form of, for example, an attached laminar boundary layer profile. The velocity gradient tensor (2.2) provides terms that can be decomposed in various ways and assembled into measures of local flow topology. One particularly relevant decomposition splits the velocity gradient tensor into three matrices: average normal, or bulk, strain rate; deviatoric strain rate; and vorticity. They are given respectively in equation 2.3 with the physical deformation corresponding to each diagram in Figure 2-1.

$$\vec{q} = \begin{bmatrix} u \\ v \end{bmatrix} \tag{2.1}$$

$$\nabla\vec{q} = \begin{bmatrix} \frac{\partial u}{\partial x} & \frac{\partial u}{\partial y} \\ \frac{\partial v}{\partial x} & \frac{\partial v}{\partial y} \end{bmatrix} \tag{2.2}$$

$$\nabla\vec{q} = \frac{1}{2}\begin{bmatrix} \frac{\partial u}{\partial x} + \frac{\partial v}{\partial y} & 0 \\ 0 & \frac{\partial u}{\partial x} + \frac{\partial v}{\partial y} \end{bmatrix} + \frac{1}{2}\begin{bmatrix} \frac{\partial u}{\partial x} - \frac{\partial v}{\partial y} & \frac{\partial u}{\partial y} + \frac{\partial v}{\partial x} \\ \frac{\partial u}{\partial y} + \frac{\partial v}{\partial x} & \frac{\partial v}{\partial y} - \frac{\partial u}{\partial x} \end{bmatrix} + \frac{1}{2}\begin{bmatrix} 0 & \frac{\partial u}{\partial y} - \frac{\partial v}{\partial x} \\ \frac{\partial v}{\partial x} - \frac{\partial u}{\partial y} & 0 \end{bmatrix} \tag{2.3}$$

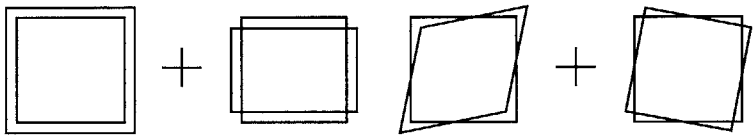

Figure 2-1: Elemental deformation decomposition

The entries of each component matrix provide a scalar magnitude of that component's physical presence. The values of the entries in the bulk normal strain and vorticity matrices are invariant with coordinate rotation. In the case of the deviatoric strain rate matrix, normal strain components are in the diagonal entries and pure shear components lie in the off-diagonal entries. Deviatoric normal strain and pure shear strain are themselves mechanically identical and interchangeable via coordinate rotation. Fundamentally, the interchangeability is due to the fact that the

strain matrix is a tensor and therefore invariant with coordinate transformation [24]. The invariant quantity of relevance for the deviatoric matrix is in equation 2.7, as developed in the following discussion.

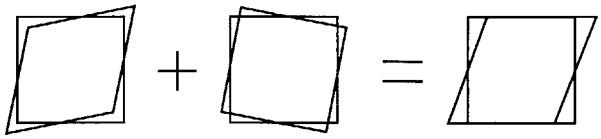

Figure 2-2: Elemental simple shear decomposition

Figure 2-2 demonstrates that approximately equal portions of deviatoric strain and vorticity comprise a simple shear element typical of a boundary layer. The bulk strain rate is irrelevant to shear flows, so it should be ignored. Deviatoric strain can take place in inviscid as well as viscous portions of the flow, such as inviscid flow in a converging channel, so the deviatoric cannot be used alone for shear layer identification.

The vorticity vector is in the out-of-plane direction with a magnitude ω (2.5) given by its off-diagonal entry. In a similar manner, and keeping in mind that deviatoric normal strain and pure shear strain are mechanically identical, Equation 2.7 shows how the diagonal and off-diagonal entries of the deviatoric matrix produce $\bar{e}$, which we choose to call the deviatoric. $\bar{e}$ is the scalar measure of deviatoric strain.

$$\bar{\bar{\omega}} \equiv \begin{bmatrix} 0 & \frac{\partial u}{\partial y} - \frac{\partial v}{\partial x} \\ \frac{\partial v}{\partial x} - \frac{\partial u}{\partial y} & 0 \end{bmatrix} \tag{2.4}$$

$$\omega = \left| \frac{\partial v}{\partial x} - \frac{\partial u}{\partial y} \right| \tag{2.5}$$

$$\bar{\bar{e}} \equiv \begin{bmatrix} \frac{\partial u}{\partial x} - \frac{\partial v}{\partial y} & \frac{\partial u}{\partial y} + \frac{\partial v}{\partial x} \\ \frac{\partial u}{\partial y} + \frac{\partial v}{\partial x} & \frac{\partial v}{\partial y} - \frac{\partial u}{\partial x} \end{bmatrix} \tag{2.6}$$

$$\bar{e} = \sqrt{\left(\frac{\partial u}{\partial x} - \frac{\partial v}{\partial y} \right)^2 + \left(\frac{\partial u}{\partial y} + \frac{\partial v}{\partial x} \right)^2} \tag{2.7}$$

The vorticity scalar is an enticing measure of "boundary layerness." It turns out that vorticity shares many of entropy's drawbacks of manifestation in other flow regions besides shear layers, not the least of which is freestream vorticity in three-dimensional flows. A quantity that represents simple shear should be greatest wherever $\omega = \bar{e}$ and smallest wherever one or both components are small. The simple shear quantity (2.8) includes viscosity to reflect the physical mechanism behind shear layers. When addressing a simple shear element like that in Figure 2-2, with the x-axis horizontal and the y-axis vertical, the quantity reduces to $\mu\frac{\partial u}{\partial y}$, which is the force per unit area due to viscous shear.

$$\textit{simple shear rate} \sim \mu\sqrt{\bar{e}\omega} \tag{2.8}$$

Although the simple shear measure is tuned to the elemental structure of shear layers, it still contains some ambiguity. For instance, given two flat plates separated by a film of fluid, with one plate moving steadily over the other, the entire velocity profile through the film looks like a simple shear element, and yet there is no distinguishable edge. The fundamental flaw in all *local* topological measures is that shear layers are *regionally* distributed flow features. When an observer qualitatively identifies a shear layer from a velocity vector field, the intuitive indicator is a velocity profile. The shear layer edge is located where the layer's velocity profile blends into the freestream. Locally all kinds of variabilities can appear in the velocity gradient tensor, particularly in unsteady flows (including DNS and LES flows). It appears to be impossible, in general, to observe the state of the flow at a particular point and make a positive determination as to whether the point is inside of a shear layer or not. A universally applicable shear detector must incorporate regional information about the flow topology.

Distinct Convected Detector Solution

The core principle of the work presented in this thesis is found in the synthesis of a flowfield measure, targeted specifically at shear layers, with the implementation of

that measure as the source term in a convection equation. The physical picture is that strong shear layer flows participate the most in the generation of the detector term, which then convects downstream to color all weaker portions of boundary layer and wake flow. The detector term effectively becomes a new fluid property, something along the lines of the degree of shear influence upon the flow. Such an arrangement bears considerable similarity to physical properties like entropy with the caveat that the source term is more selective. Molecular diffusion, such as would occur with smoke in a wind tunnel, is not a part of our model due to the already diffuse nature of shear layers. The conservation equation takes the following form, where Σ is the source term, dependent on the local state of the flow, and χ is the detector variable. The source term units determine those of the detector variable.

$$\frac{D\chi}{Dt} = \Sigma \tag{2.9}$$

Multiplying by ρ and expanding,

$$\rho\frac{\partial\chi}{\partial t} + \rho\vec{q}\cdot\nabla\chi = \rho\Sigma \tag{2.10}$$

Using the fact that all of the terms in the mass conservation equation 2.11 add to zero, we arrive at the numerically conservative form of the detector equation 2.13.

$$\frac{\partial\rho}{\partial t} + \nabla\cdot(\rho\vec{q}) = 0 \tag{2.11}$$

$$\rho\frac{\partial\chi}{\partial t} + \rho\vec{q}\cdot\nabla\chi + \chi\left[\frac{\partial\rho}{\partial t} + \nabla\cdot(\rho\vec{q})\right] = \rho\Sigma \tag{2.12}$$

$$\frac{\partial(\rho\chi)}{\partial t} + \nabla\cdot(\rho\chi\vec{q}) = \rho\Sigma \tag{2.13}$$

The primary difficulty remaining is the choice of source term, an issue left to the subsequent section on detector formulations (Section 2.2). The detector variable has a zero or near-zero value in the freestream with an iso-surface threshold marking say δ_{99}. An additional benefit of such a detector is the characterization of the amount of

shear influence within shear layers, information that finds application in visualization and grid adaptation. The computational cost of solving for a new differential equation is accepted as necessary for a generalized shear layer detector.

The convection equation is hyperbolic. With respect to boundary conditions, the inflow value of the detector scalar is set to a uniform zero value, corresponding to "clean" inflow. On a wall the normal velocity component is zero, so although no boundary condition is explicitly set, the flux through the wall is zero. No condition is applied at outflow.

Steady recirculation regions may present some difficulties for the convection equation in that their closed streamlines isolate them from the remainder of the flow. That said, given that the shear layer extraction technique locates the edge of the boundary layers, wakes, and so forth in the flow, recirculation zones will either be fully enclosed within the edge surface or excluded beyond it. Recirculation zones will not disturb the continuous shear layer edge surface. We press on with the implementation of a convection-based shear layer feature extraction tool.

2.1.3 Prior Work

CFD investigators currently use feature extraction tools developed for vortex cores and shock surfaces. To date no comparably successful shear layer tool exists. The proposed convective extraction method uses much of the same reasoning and methodology as turbulence models, although turbulence modeling differs somewhat in its goals and methods. A paper was published covering the beginning of the work for this thesis [3].

Turbulence Models

Turbulence models for Reynolds-averaged viscous flows often require knowledge of shear layer edge information, or at least knowledge of a particular element's location within a shear layer. Many algebraic models and one-equation turbulence models, such as the Cebeci-Smith model [6], require an estimate of the boundary layer edge

location. The Baldwin-Lomax model [2] bypasses this particular difficulty but still makes use of velocity profile information along a path normal to the surface, as do many other turbulence models. The dependence upon geometry brings to bear the difficulties discussed in Section 2.1.1 on line integration.

As a minimum, turbulence models must determine whether to act on the solution, a determination that still requires knowledge of where shear layers exist. The most generally applicable models, perhaps the most popular of which is the Spalart-Allmaras model [23], almost always use vorticity as a basis to describe shear layer information [11], an approach that works adequately in many flows but contains inaccuracies mentioned previously in the section on local state properties. The goals of turbulence models are also different from a shear detector in that they seek to alter the solution rather than simply measure it.

Let us take a closer look at the Spalart-Allmaras model in particular from the perspective of mining it for shear layer detection ideas. Its core equation (2.14) for the dynamic eddy viscosity ν_t (directly dependent upon the working variable $\tilde{\nu}$) closely resembles the shear detector convection equation.

$$\begin{aligned}\frac{D\tilde{\nu}}{Dt} &= c_{b1}[1-f_{t2}]\tilde{S}\tilde{\nu} \\ &+\frac{1}{\sigma}\left[\nabla\cdot((\nu+\tilde{\nu})\nabla\tilde{\nu})+c_{b2}(\nabla\tilde{\nu})^2\right]-\left[c_{w1}f_w-\frac{c_{b1}}{\kappa^2}f_{t2}\right]\left[\frac{\tilde{\nu}}{d}\right]^2+f_{t1}\Delta U^2\end{aligned} \tag{2.14}$$

The first term on the right-hand side is the driving production term, where $\tilde{S}$ depends upon the vorticity magnitude. The remaining terms are for diffusion, destruction pertaining to log layer accuracy, and tripping from laminar to turbulent flow, respectively. The freestream value of $\tilde{\nu}$ is 0, as is the wall boundary value, unlike what would be desirable for a general shear detector. The destruction and diffusion terms, while useful for matching time-averaged turbulent boundary layer profiles, may not be so useful for catching shear effects in general. The complexity of the model indicates that it may be necessary for a shear detector to actively distinguish between laminar and turbulent flows.

Dedicated Detectors

A thesis by Lovely [19] focuses on finding integrated boundary layer thicknesses based upon the geometry of the simulation. The implementation requires the construction of integration paths as described in Section 2.1.1 and employs integration of vorticity to determine boundary layer thicknesses. It demonstrates excellent accuracy when finding boundary layer quantities for simple flow geometries in two dimensions. Because it is sensitive to freestream vorticity, difficult to apply to wakes, and computationally expensive, it proved to be impractical for arbitrary geometries and unsteady simulations.

A convective approach specific to feature extraction was originally implemented by Haimes for the identification of recirculation regions [12]. It tracks the residence time of each element of the flow and isolates the portion of the flow that lingers within the domain. Haimes also explored local velocity gradient tensor indications of shear flow via eigenvalue analysis [14], work partly described in the section on topological issues (Section 2.1.2).

2.2 Shear Detector Formulations

2.2.1 Navier-Stokes Equations Viscous Terms Source

One intuitive idea for how to locate shear layers is to calculate the inviscid flow for the same geometry and flow conditions and then label the regions that do not match as shear layers. Though the influence of viscosity upon a flow's behavior makes this idea unrealistic, it is useful to consider such a concept instead in terms of the flow equations themselves. To this end we can take the difference between the Euler (2.15) and Navier-Stokes (2.16) momentum equations to be a gauge of viscosity's influence upon the flow. The vector magnitude of the Navier-Stokes momentum equation's viscous terms forms a source term for the shear detector convection equation. To maintain consistency with any turbulence model that may be active in the simulation, within the stress tensor $\bar{\bar{\tau}}$ the viscosity μ is composed of the sum of laminar and

eddy viscosities. The choice of the second viscosity λ is actually important to the evaluation of the source term (see Section 3.2.1). With this source term, χ has units of velocity. The Navier-Stokes viscous terms formulation is pursued extensively in this investigation.

$$\frac{\partial(\rho\vec{q})}{\partial t} + \nabla \cdot [(\rho\vec{q})\vec{q}] + \nabla p = 0 \tag{2.15}$$

$$\frac{\partial(\rho\vec{q})}{\partial t} + \nabla \cdot [(\rho\vec{q})\vec{q}] + \nabla p = \nabla \cdot \bar{\bar{\tau}} \tag{2.16}$$

$$\nabla \cdot \bar{\bar{\tau}} = \frac{\partial}{\partial x_j}\left[\mu\left(\frac{\partial q_i}{\partial x_j} + \frac{\partial q_j}{\partial x_i}\right) + \delta_{ij}\lambda\nabla \cdot \vec{q}\right] \tag{2.17}$$

$$\rho\Sigma \equiv \|\nabla \cdot \bar{\bar{\tau}}\| \tag{2.18}$$

2.2.2 Velocity Gradient Tensor Quantities Source

In the discussion on topological shear indicators, it was mentioned that a combination of vorticity and deviatoric shear scalars came close to characterizing shear layers. Taken alone, this measure quantifies simple shear but does not fully address the structure of shear layers. As mentioned in Section 2.1.2, although two plates steadily sliding past each other with a viscous fluid in between them create simple shear in the fluid, in such a scenario there is no distinguishable shear layer. Recognition of the fact that shear layers can be further characterized as regions of shear *gradients* leads to a source term dependent upon the gradient of a simple shear measure. The combined vorticity/deviatoric measure, contextualized by the taking of its gradient, eliminates compressibility influence explicitly and should therefore target shear layer structure at the exclusion of other flow topologies. An important feature of the source term (2.19) is that, for the case of a simplified laminar boundary layer profile composed only of elemental simple shear, it reduces to $\frac{\partial}{\partial y}\left(\mu\frac{\partial u}{\partial y}\right)$ (absent a factor of density), just like the Navier-Stokes source term. The resultant scalar χ in the convection equation

has units of density times velocity, which is specific momentum. The units reflect the fact that viscous shear influences the momentum of the flow.

$$\rho\Sigma \equiv \rho\left|\nabla\left(\mu\sqrt{\omega\bar{e}}\right)\right| \tag{2.19}$$

2.2.3 Hypothesized Applicability

Because all shear effects are to be included by the shear detector, a single all-encompassing three-dimensional boundary layer thickness definition is desired. Once the detector proves itself reliably against known test cases, it should be able to identify the edge of shear regions for any given flow solution. A convection-based detector shows promise for meeting most of the stated ideals for a shear layer extraction tool. Once the convection equation is non-dimensionalized, it is hypothesized that the detector threshold for the shear layer edge will be invariant across a variety of flow conditions, most significantly Reynolds number and Mach number.

Chapter 3

Two-Dimensional Implementation and Verification

3.1 Implementation

3.1.1 Flow Solver

The CFD code employed in this portion of the investigation is a modification of a simple finite volume solver written by Ali Merchant [20]. While the original code solved the compressible Euler equations, the extended and revised code operates on the compressible Navier-Stokes equations as well as the shear layer detection equation to be tested. The state vector of conservative variables $\vec{U}$ is composed from primitive variables: density ρ, x- and y-velocity u and v, and total specific energy E, with the shear detector variable χ added on. Non-dimensionalization uses the following parameters: reference length L_{ref}, freestream density ρ_∞, freestream speed of sound c_∞, and freestream viscosity μ_∞.

$$\vec{U} = \begin{bmatrix} \rho \\ \rho u \\ \rho v \\ \rho E \\ \rho \chi \end{bmatrix} \tag{3.1}$$

The equations for the perfect gas law and Sutherland's law are also applied. In applying the non-dimensionalization, the sole changes are that the terms in $\bar{\bar{\tau}}$ gain a factor of $1/Re$, and that the velocity gradient tensor source likewise becomes $(1/Re)\Sigma$.

The system of equations is discretized explicitly in time using a Runge-Kutta multi-stage scheme. The flow is modeled in a quasi-steady manner with local time stepping. The equations are discretized in space using a Jameson finite volume scheme, which decouples adjacent nodes. The spatial discretization requires second-order smoothing to capture shocks and damp discontinuities and fourth-order smoothing to attenuate and stabilize numerical sawtooth oscillations [16].

Stability and Smoothing

> *In fluid dynamics you have to smooth whatever you can, whenever you can, as much as you can.*
>
> A. Jameson, 1994 [28]

Smoothing turned out to be a critical issue, particularly for the shear detector variable. The goal is to add as much smoothing as possible without excessively distorting the solution. It is a fine line to walk, and just how fine a line it is depends upon the equations in question. In the case of the Navier-Stokes equations there is adequate middle ground. Slight sawtooth oscillations remain in places where the variables trail off asymptotically, which unfortunately includes the edge of the boundary layer where it is most desirable for the shear detector to be smooth.

For the shear detector equation it was found that the degree of fourth-order smoothing necessary for stabilization was already enough to significantly influence the solution. In effect, the fourth-order constant could shift the shear layer edge

value of χ. The shear detector equation employs smoothing constants independent from the constants used for the rest of the equations so that they can be adjusted separately. Too much fourth-order dissipation actually destabilizes the shear detector equation. The results in this section reflect a decision to err on the side of reduced smoothing such that it introduces as little global error as possible in the data. As a consequence, local oscillations appear in the data presented in this section. Note that these oscillations predominate in regions where χ is below the edge value, so their influence on the edge contour is minimal. Still, the oscillations in the shear detector solution at the boundary layer edge reflect the oscillations in the flow solution.

3.1.2 Mesh

The solver operates on unstructured triangular meshes in the FUN2D [1] format. In the flat plate test case, a structured-style inviscid channel flow grid generator, written by David Venditti [26], was modified to concentrate points both across the boundary layer thickness and isotropically near the plate leading edge (Figure 3-1). In the airfoil cases an unstructured viscous grid generator, also by Venditti [26], employed stretched cells near the surface to better resolve the boundary layer (Figure 3-20).

Given that the wake is of particular interest in our shear layer detector investigation, the proper modeling and resolution of its structure is essential. The unstructured airfoil grid generator used here, in line with standard practice for grid generators of this kind, does not attempt to resolve the wake. Therefore adaptive grid refinement, one of the target applications of this thesis, is introduced.

The wake refinement algorithm uses a combined measure of the shear detector concentration and the cell area to determine which cells to refine and by how much. An ellipse of exclusion around the airfoil prevents the corruption of nicely-structured cells in the boundary layer. The freely available program "Triangle" [22] carries out the actual reassignment of grid geometry. Three iterations of refinement and re-convergence of the solver are sufficient to adequately model the wake. This rudimentary refinement produces a prodigious number of cells (Figure 3-21). It could stand some improvement in the form of grid smoothing, cell stretching in the flow

direction, and a more accurately targeted and universally applicable measure for the designation of cells to refine, but it serves the purposes of this experiment.

3.1.3 Visualization

Although the quantitative testing pursued here makes use of the numerical values of the shear detector variable, as described in Section 3.2, visualization is also possible even at the earliest stages of the investigation. Flow with a shear detector value below the edge threshold is excluded, while flow with an equal or higher detector value is colored on a logarithmic scale. In this manner the investigator can visualize both the shear layer edge and the degree of shear influence within that edge.

3.2 Test Cases

Each case tests the hypothesis that an iso-surface of the shear detector variable matches the outer surface of the boundary layers and wakes present in the flow. In these two-dimensional cases, contour lines of the detector are compared to the known location of the boundary layer edge at δ_{99}. For precise quantification of how well the contours correspond with δ_{99}, samples of the detector value are taken at specific points along the known edge line. *All test case figures use the Navier-Stokes viscous terms source unless marked with "VGT," for velocity gradient tensor quantities source.*

Each test has a baseline flow condition that serves as a control. Individual test cases vary from the baseline in one variable only. *Figures represent the baseline condition unless otherwise noted.*

3.2.1 Flat Plate

The flat plate test is meant to evaluate the performance of the shear detector for the simplest possible shear layer with no other flow features. The Blasius solution [10], an analytical solution to incompressible laminar flow along a flat plate, serves as the standard of comparison.

$$\delta_{99} = \frac{5.0x}{\sqrt{Re_x}} \tag{3.2}$$

The boundary conditions for the flow solver are a symmetry condition leading up to the plate, no-slip and constant temperature at the plate, freestream conditions imposed on the flow inlet, and freestream pressure imposed at the top and the outlet with other conditions extrapolated from within the domain.

Conditions of a Reynolds number of 1×10^3 and a Mach number of 0.3 serve as the baseline case. The first batch of test cases covered a variation in Reynolds number from 5×10^2 to 1×10^4. The results demonstrated excellent agreement between a shear detector contour and the reference edge line. Figure 3-7 is a representative case, where the dashed line is the boundary layer edge. Increased smoothing can readily remedy the slight instability at the plate leading edge, again at the potential cost of accuracy loss. The source term is quite heavily concentrated in a very small region starting at the plate leading edge and extending a tiny bit downstream and out away from the plate. Figure 3-6 does not quite do the source concentration justice, since the peak value touching the plate leading edge is 3.12 on the logarithmic contour scale. The source contour blip across $x = 0$ reflects the effect of the switching grid diagonal direction. Figure 3-8 shows how the contours track well at an increased Reynolds number.

As hypothesized, nearly the same value of detector contour value corresponded to the edge line in each simulation, demonstrating the desired detector insensitivity to Reynolds number. The data in Table 3.1 shows (for the velocity gradient tensor terms source) that the detector boundary layer edge threshold χ_δ does exhibit some Reynolds number dependency. The data in Table 3.2 confirms the suspicion that source term sensitivity to grid spacing is at least partially at fault. The source term contains derivatives of quantities that themselves contain derivatives, exacerbating the effect of errors due to inadequate resolution. In Table 3.2 the vertical spacing of the grid scales with the boundary layer thickness. For both tables δ % error refers to the error in the boundary layer thickness if χ_δ from the baseline condition is used to

Table 3.1: Flat plate shear detector threshold dependence upon Reynolds number, constant grid, VGT source

Re	χ_δ	δ % error
500	0.00131	-0.8
1000	0.00140	—
5000	0.00188	4.0

Table 3.2: Flat plate shear detector threshold dependence upon Reynolds number, grid y-axis scaling with $1/\sqrt{Re}$, VGT source

Re	χ_δ	δ % error
500	0.00136	-0.4
1000	0.00140	—
5000	0.00160	2.2

represent the boundary layer edge at other flow conditions.

Based upon the accuracy of the solver at different dissipation levels, as presented in Figure 3-9, the flow equation dissipation constants were set at 0.005 for second-order and 0.05 for fourth-order. The shear detector dissipation constants were set very low at 0.001 each. Note that the flow speed-up seen in the contours above the boundary layer in Figures 3-3 and 3-5, as well as in the profile plot in Figure 3-10, does not effect the boundary layer edge position, just its edge speed. The speed-up phenomenon is physically correct. The Blasius profile does not reflect it due to the assumption of pressure uniformity in the freestream. Profiles represent the flow at $x/L = 0.5$. Figures 3-11 and 3-12 show how the source and detector terms, respectively, vary through the boundary layer, where δ_{99} is at $y/L = 0.111$.

The next set of tests covered a range of Mach numbers from 0.3 to 0.7 at the baseline Reynolds number of 1×10^3. This time, in comparing Figures 3-7 and 3-13, the results belie a slight detector sensitivity to Mach number. In the dependency plot in Figure 3-14, the sensitivity looks high, but because the contours vary logarithmically in space, a moderate change in contour value means only a small change in physical location. Some error likely stems from compressibility effects for which the Blasius

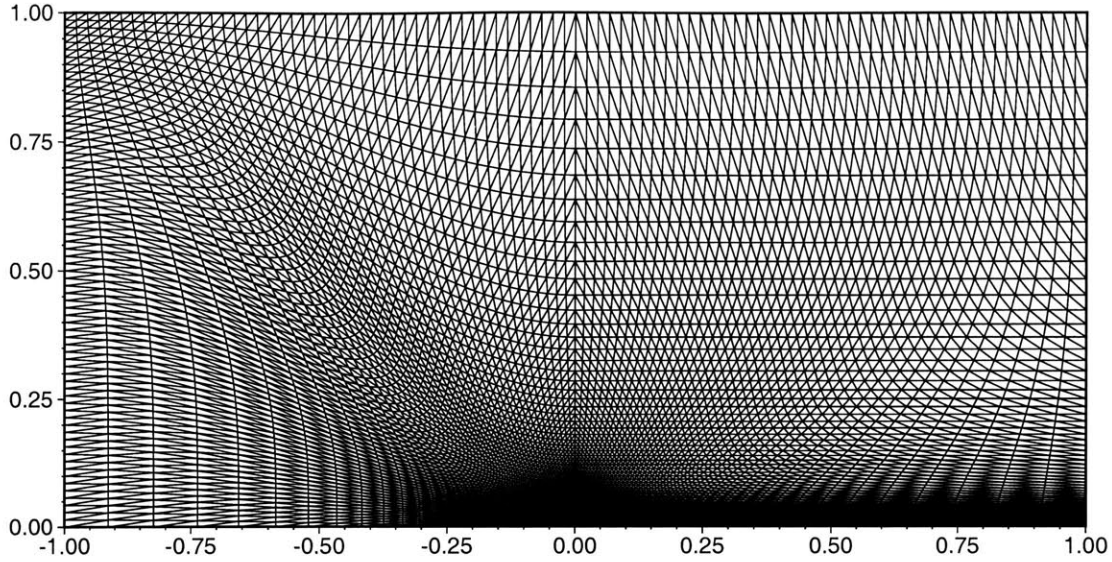

Figure 3-1: Flat plate computational grid

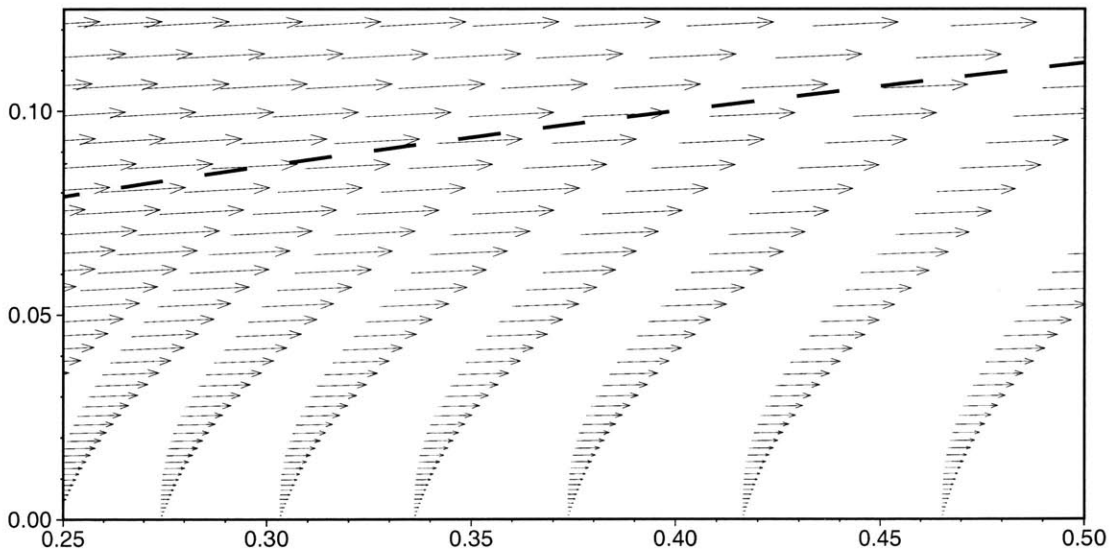

Figure 3-2: Flat plate boundary layer velocity vector field

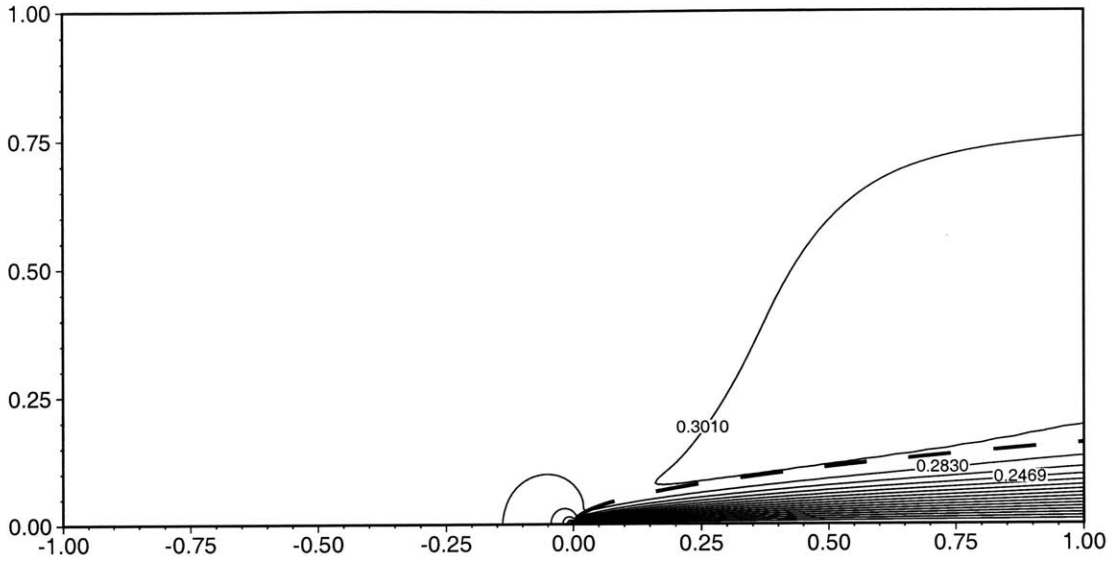

Figure 3-3: Flat plate u/c_∞ contours

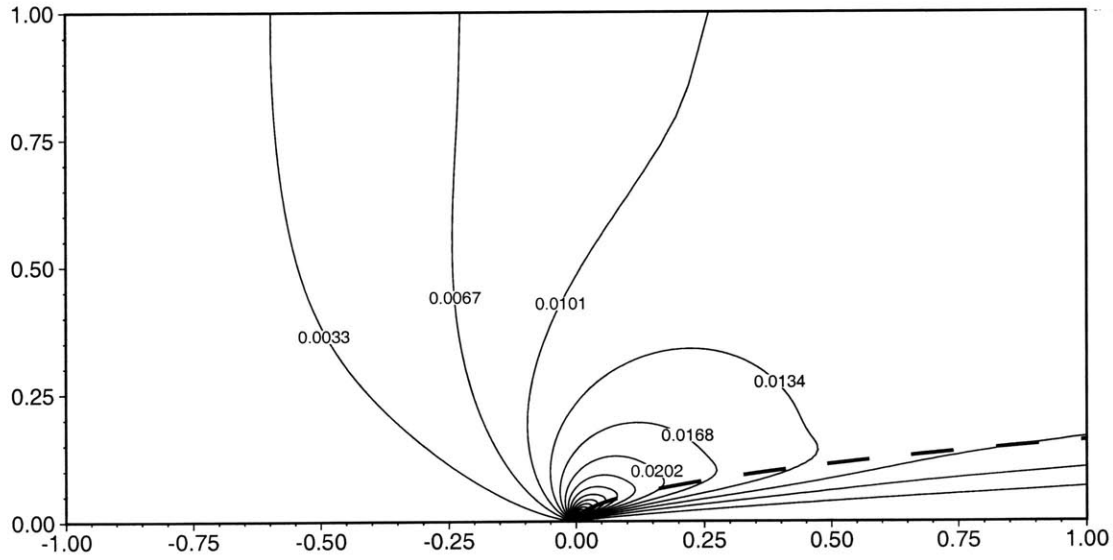

Figure 3-4: Flat plate v/c_∞ contours

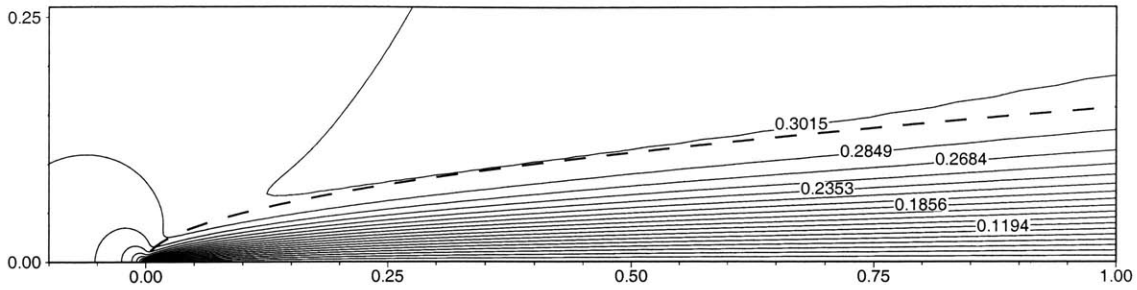

Figure 3-5: Flat plate Mach number contours

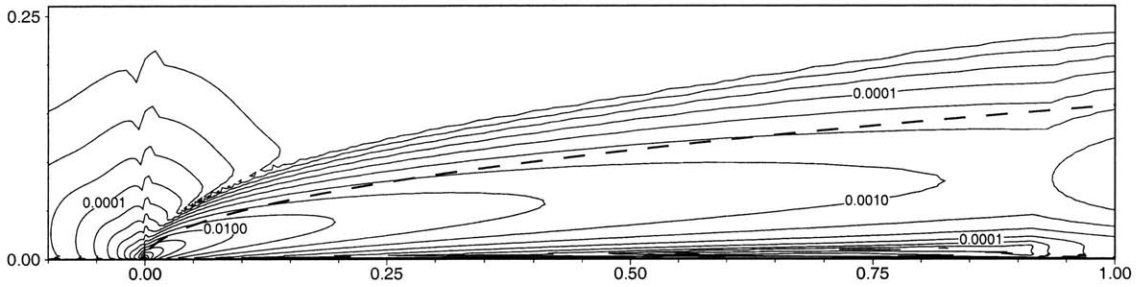

Figure 3-6: Flat plate Σ contours (exponential scale)

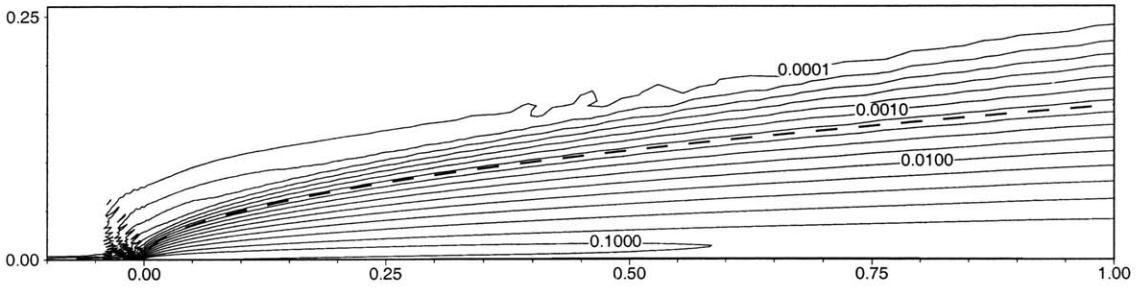

Figure 3-7: Flat plate χ contours (exponential scale)

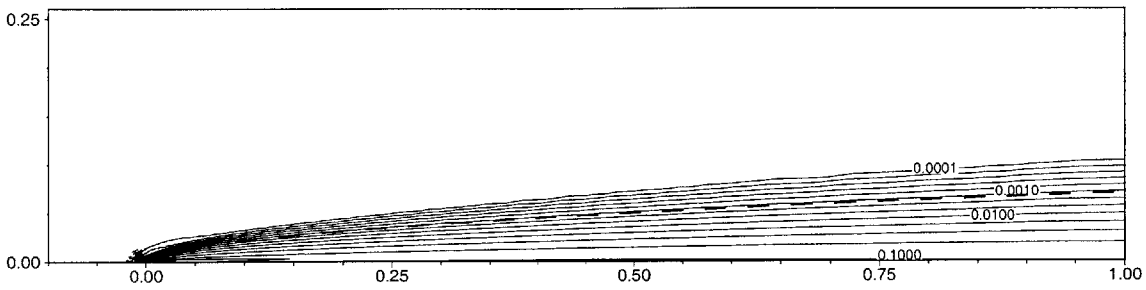

Figure 3-8: Flat plate χ contours (exponential scale), $Re = 5 \times 10^3$

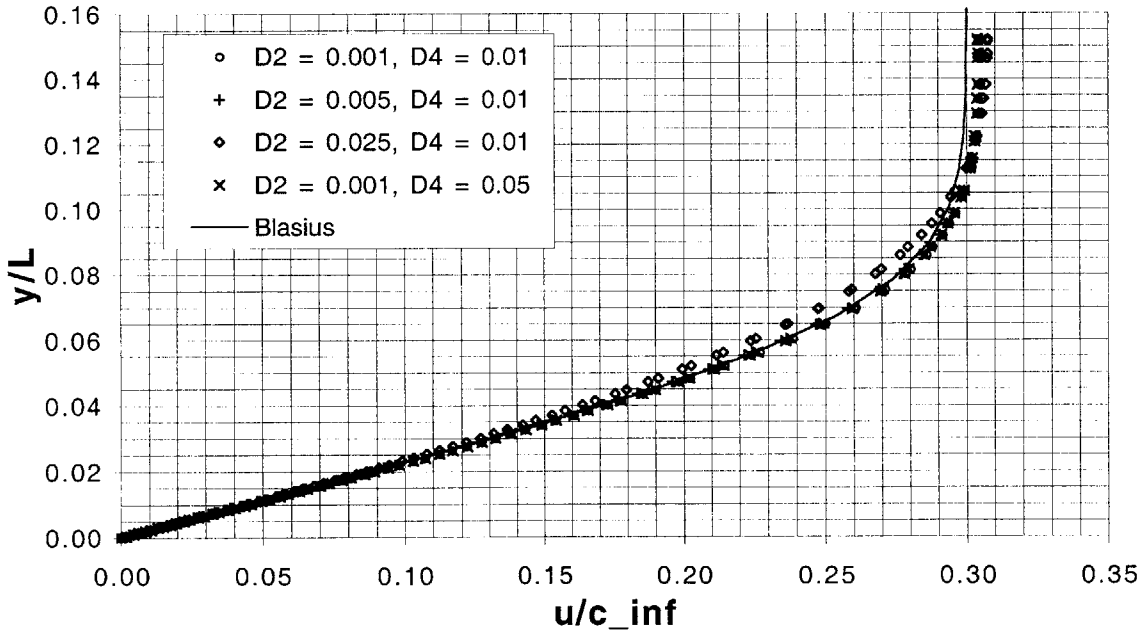

Figure 3-9: Flat plate velocity profile dependence upon dissipation constants

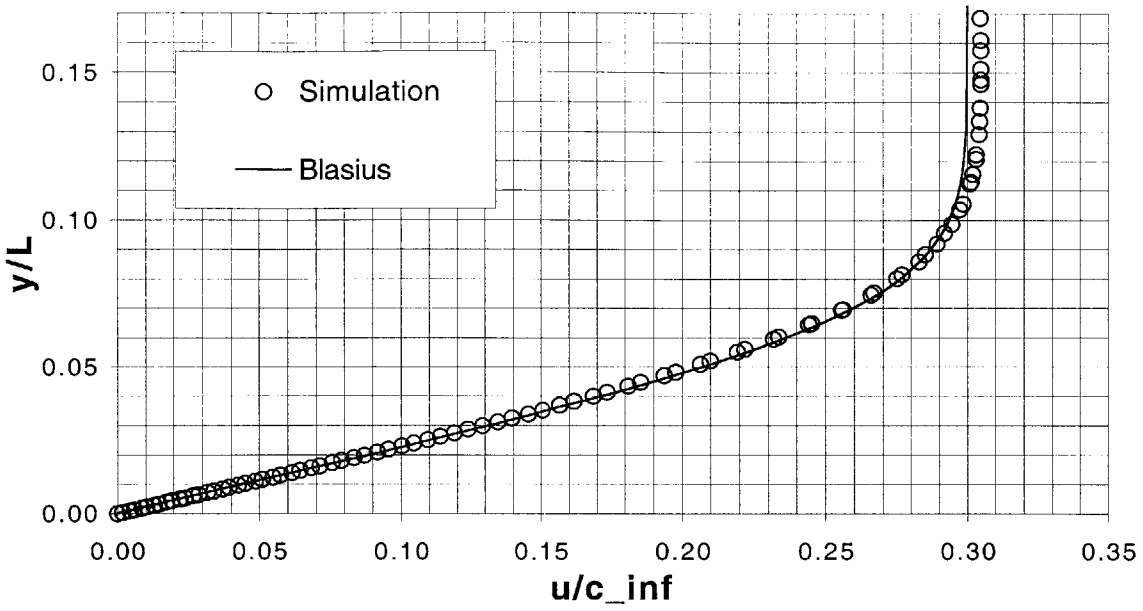

Figure 3-10: Flat plate velocity profile verification against Blasius solution

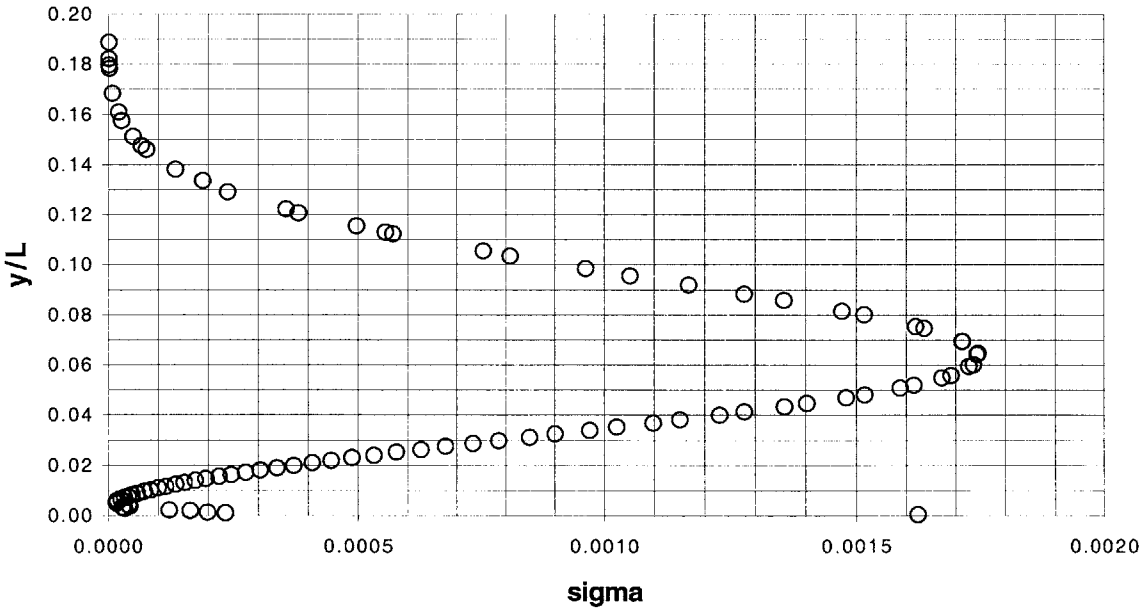

Figure 3-11: Flat plate Σ profile, $\delta_{99} = 0.111$

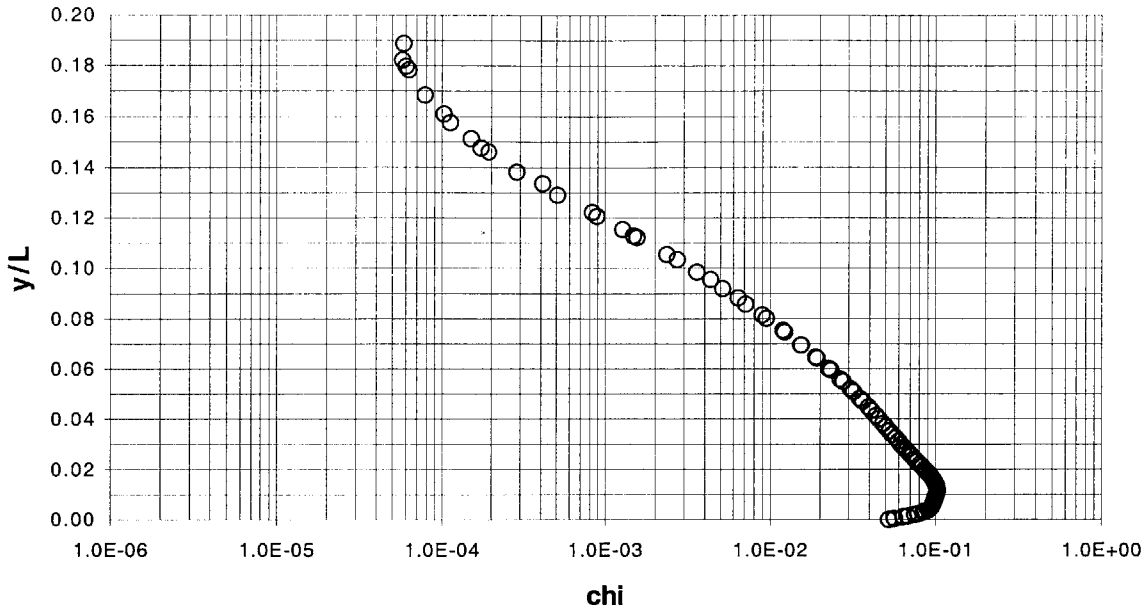

Figure 3-12: Flat plate χ profile, $\delta_{99} = 0.111$

solution does not account.

The contours again lie nicely parallel to the edge line, but the contour value corresponding to that line appeared to bear an exponential or power-law relationship to the Mach number. It is possible that this effect stems from an unanticipated compressibility effect on the source term. The detector variation with Mach number bears similarities to that of drag force. In Figure 3-14, the example trendline is a 2nd order polynomial. Interestingly, even though the divergence of the velocity is small, the Stokes hypothesis of $\lambda = -(2/3)\mu$ proved important. When the second viscosity λ is neglected, the contours near the plate leading edge are depressed below the boundary layer edge and do not follow it as well.

The same tests, when repeated using the velocity gradient tensor terms source, yielded similar results. As can be seen from Figure 3-19, the Mach dependency is nearly identical, which is surprising given that bulk expansion has been removed from the source term. However, Reynolds number dependency as given in Tables 3.1 and 3.2 is reduced from that of the Navier-Stokes source. Also, the velocity gradient tensor source does not pick up as much of the flow above the boundary layer leading

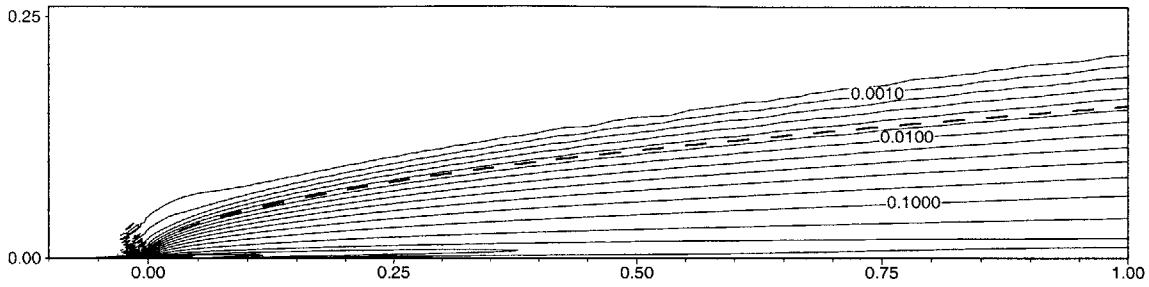

Figure 3-13: Flat plate boundary layer χ contours (exponential scale), $M = 0.7$

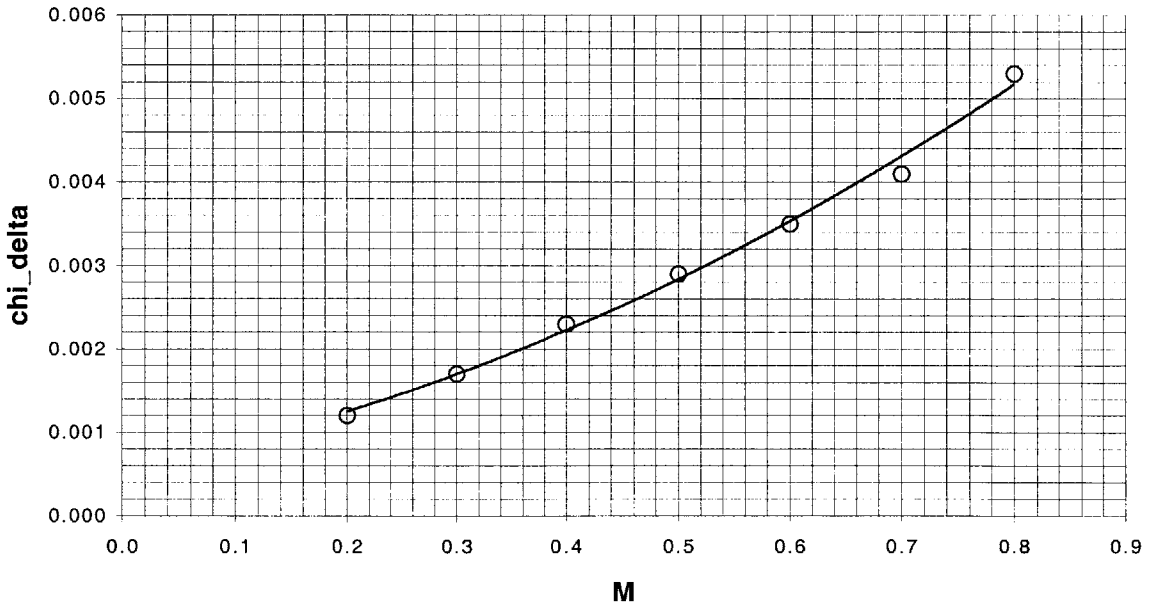

Figure 3-14: Flat plate χ edge threshold Mach dependence

edge (Figure 3-15), a trait that is desirable for reducing spurious boundary layer indications. It is still the case that the source term is heavily concentrated at the plate leading edge.

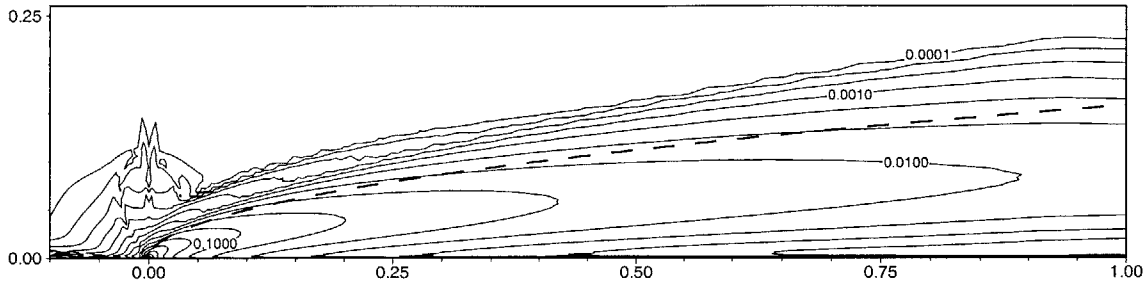

Figure 3-15: Flat plate VGT Σ contours (exponential scale)

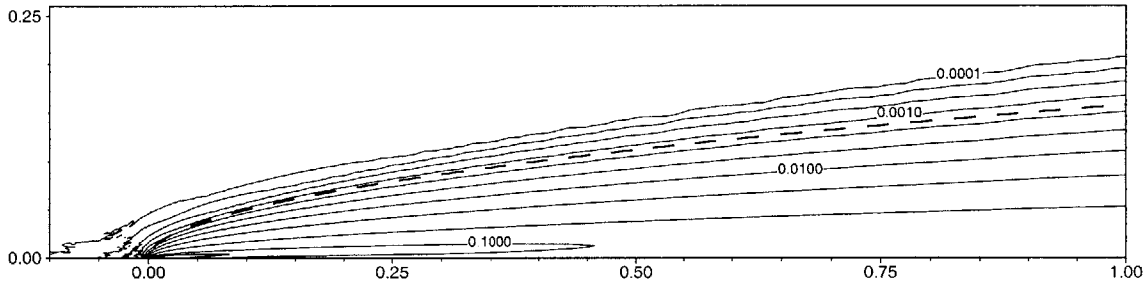

Figure 3-16: Flat plate VGT χ contours (exponential scale)

3.2.2 NACA 0005 Airfoil

The purpose of this laminar, fully attached flow test case is to assess the accuracy of the shear detector in a flowfield that is within the typical range of complexity for engineering simulations. At low angles of attack, the boundary layers on the thin NACA 0005 airfoil remain laminar and attached at relatively large Reynolds numbers. This trait provides a wide Reynolds number range for physically meaningful test simulations, given the solver's lack of a turbulence model. In this test the reference shear layer edge line is given by MSES [7], a well-established airfoil flow modeling program (see Section 1.2.2). The program operates on boundary layer parameters

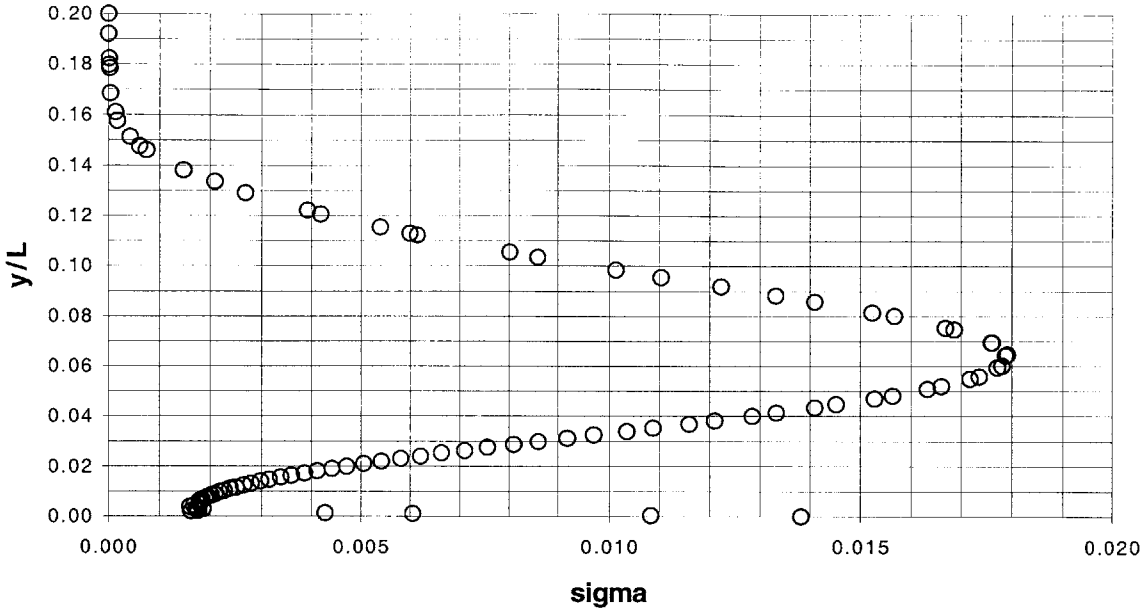

Figure 3-17: Flat plate VGT Σ profile, $\delta_{99} = 0.111$

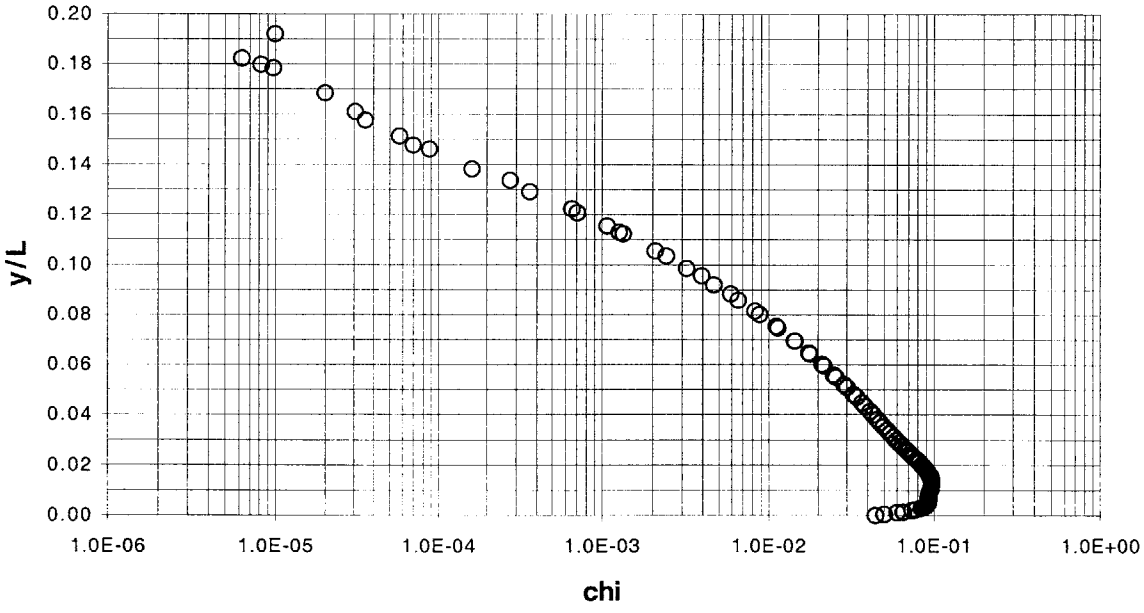

Figure 3-18: Flat plate VGT χ profile, $\delta_{99} = 0.111$

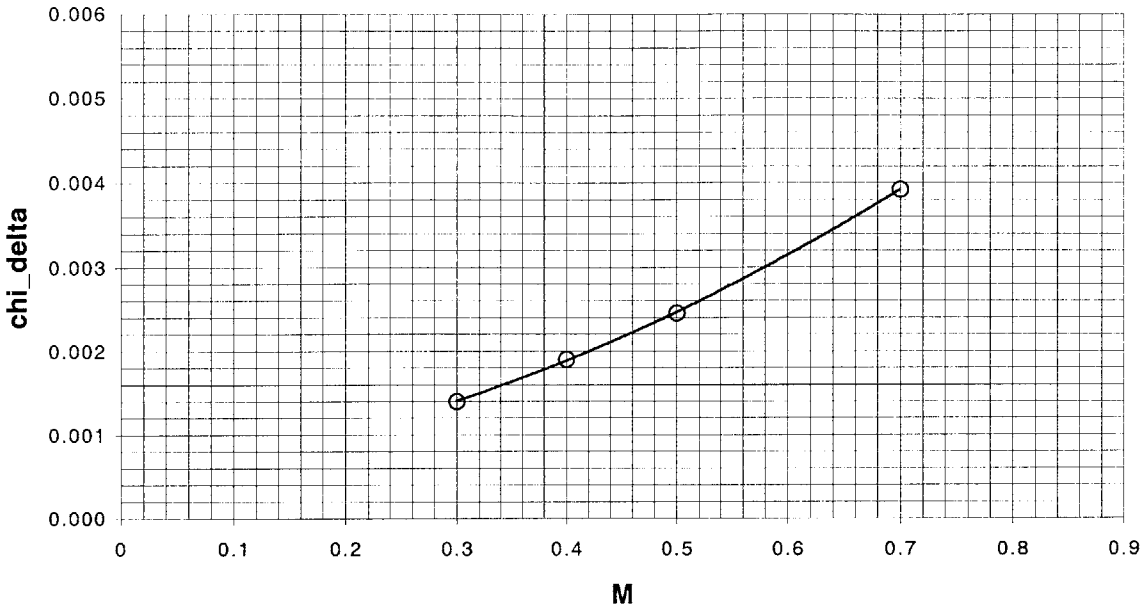

Figure 3-19: Flat plate VGT χ edge threshold Mach dependence

directly, so with some manipulation it was made to output coordinates for the shear layer edge line. Although wakes generally tend to be turbulent in real flows under the chosen conditions, the laminar Navier-Stokes code demands a laminar standard of comparison. Therefore it is necessary to modify MSES to eliminate the assumption that the wake flow is turbulent. Efforts in that direction were not successful, so no direct standard of comparison is presented for the wake.

As in the flat-plate tests, the Navier-Stokes flow solver uses a no-slip, constant temperature boundary condition on the surface of the airfoil. The accuracy of the farfield boundary conditions is improved with a source/vortex model. The baseline flow conditions are $M = 0.3$, $Re = 1 \times 10^4$, and angle of attack $\alpha = 1.5$ degrees. As stated before, the grid refinement algorithm resolved the wake flow structure in three convergence stages (compare Figures 3-20 and 3-21). Figure 3-23 demonstrates the retention of the boundary layer cell structure. Each refinement stage required 2000 to 10000 iterations, the first and last grids taking the longest.

The Mach contours compare well with MSES (Figures 3-25 and 3-26). Note that the MSES model represents the boundary layer with a displacement surface and does

not directly provide velocity contours for the boundary layer and wake. On the plots, the set of dashed lines closer to the airfoil centerline denotes the displacement surface, given here merely for reference, and the outer set of lines denotes the shear layer edge. Shear detector contours matched boundary layer edge lines well in all cases. The contour value corresponding to the edge demonstrated the desired insensitivity to Reynolds number, demonstrated by Figures 3-28 and 3-29, as well as to angle of attack. The edge contour also corresponds to the same flow conditions in the flat plate case. Once again, in comparing Figures 3-28 and 3-30, some Mach dependency appeared. The example visualizations in Figures 3-31 and 3-32 vividly demonstrate the ease with which the observer can detect variations in boundary layer behavior.

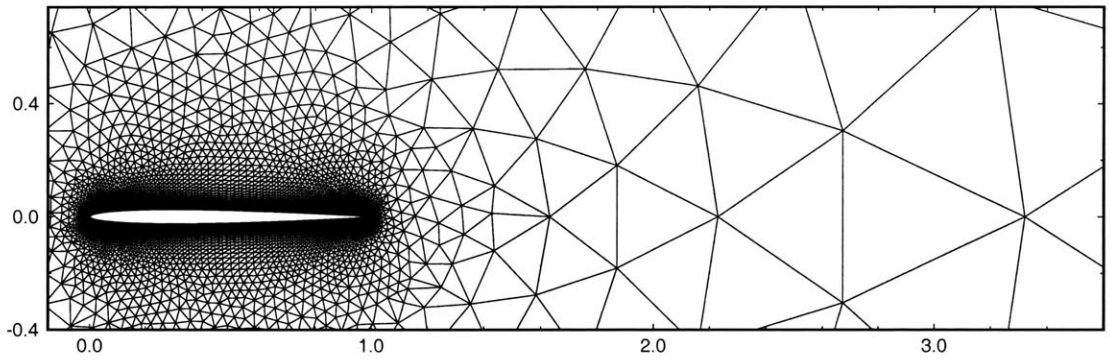

Figure 3-20: NACA 0005 original computational grid

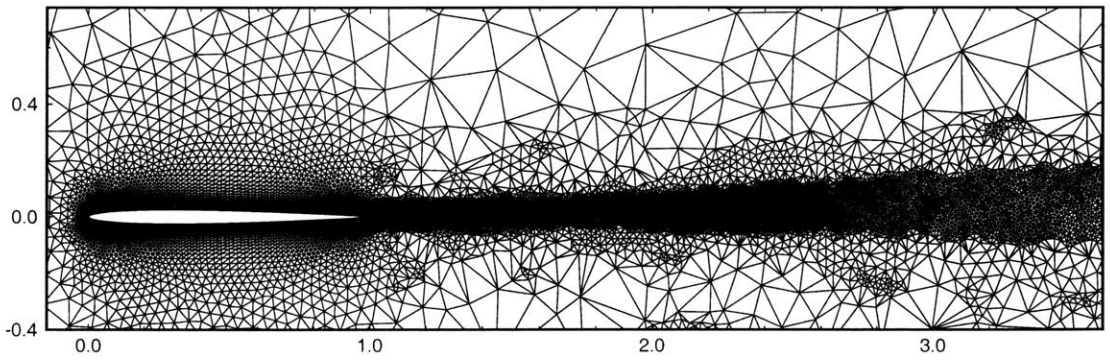

Figure 3-21: NACA 0005 refined computational grid

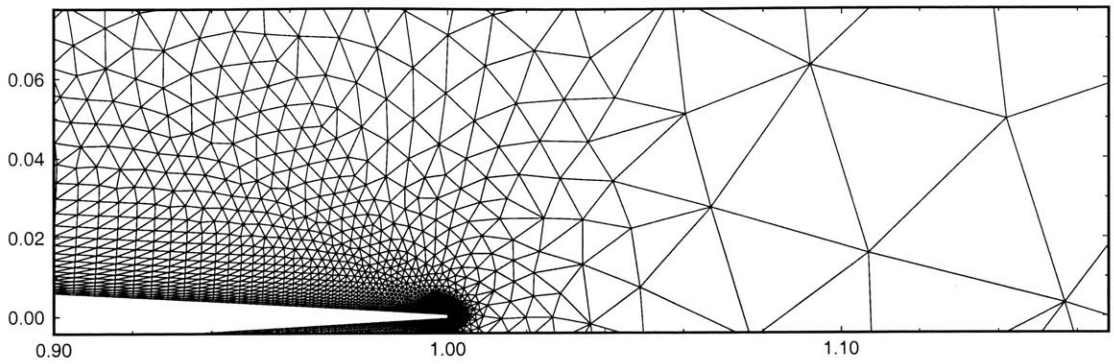

Figure 3-22: Original grid trailing edge

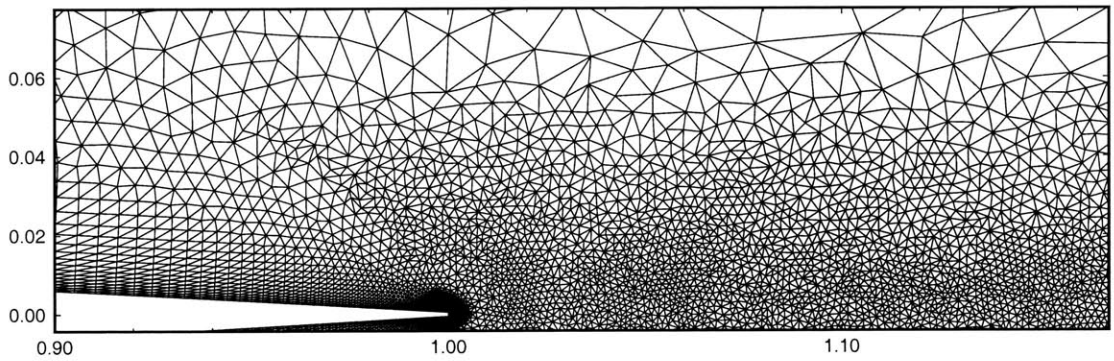

Figure 3-23: Refined grid trailing edge

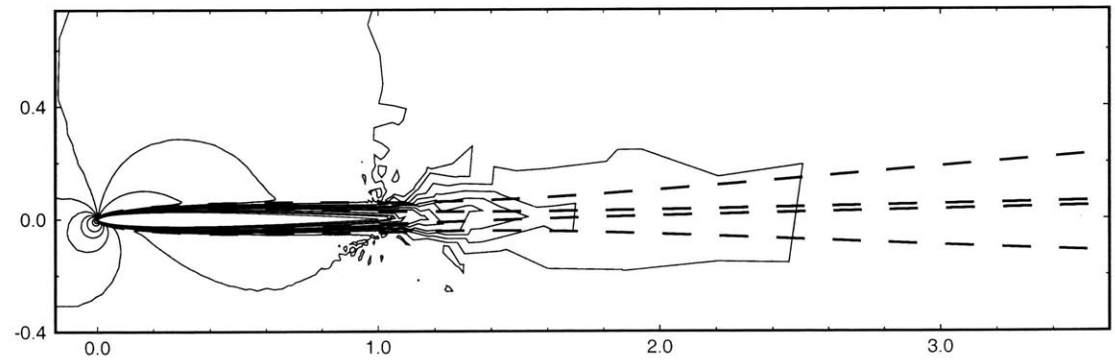

Figure 3-24: Mach contours, original grid

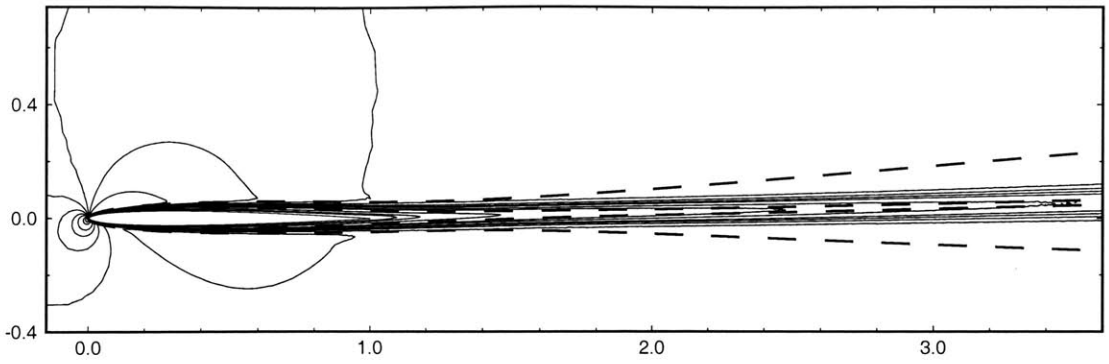

Figure 3-25: Mach contours, refined grid

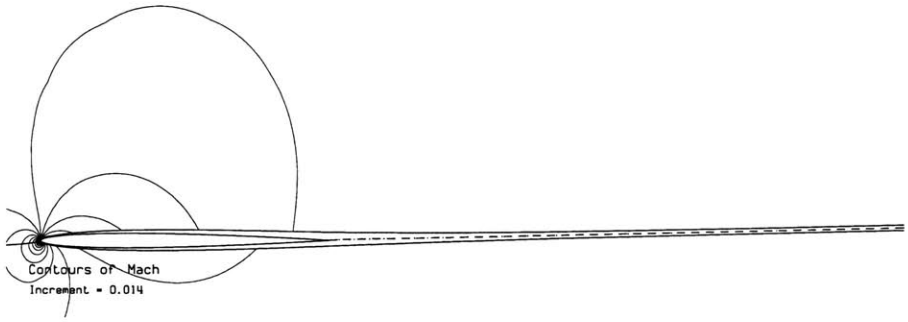

Figure 3-26: Mach contours using MSES

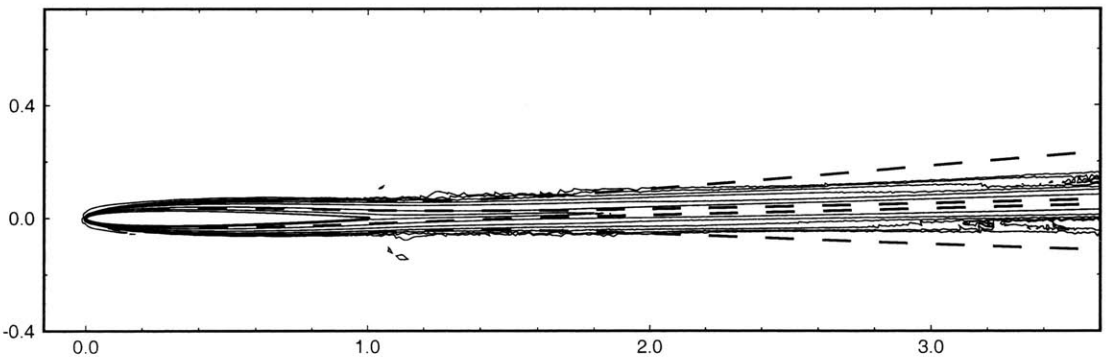

Figure 3-27: χ contours

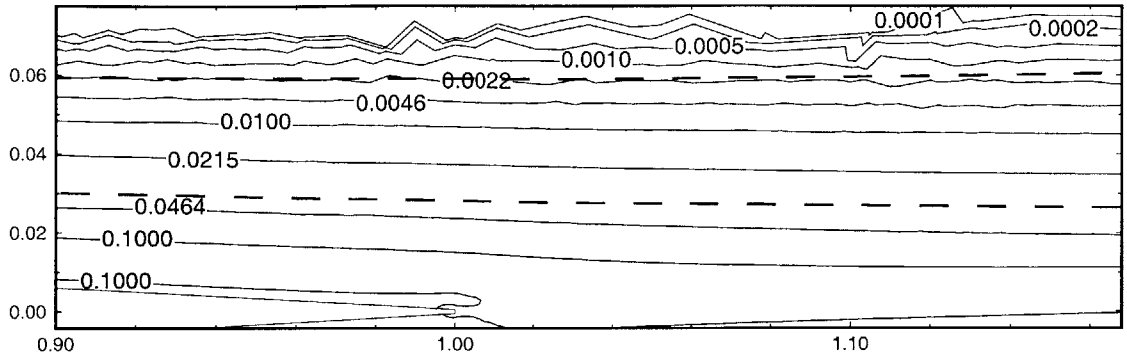

Figure 3-28: χ contours, trailing edge detail

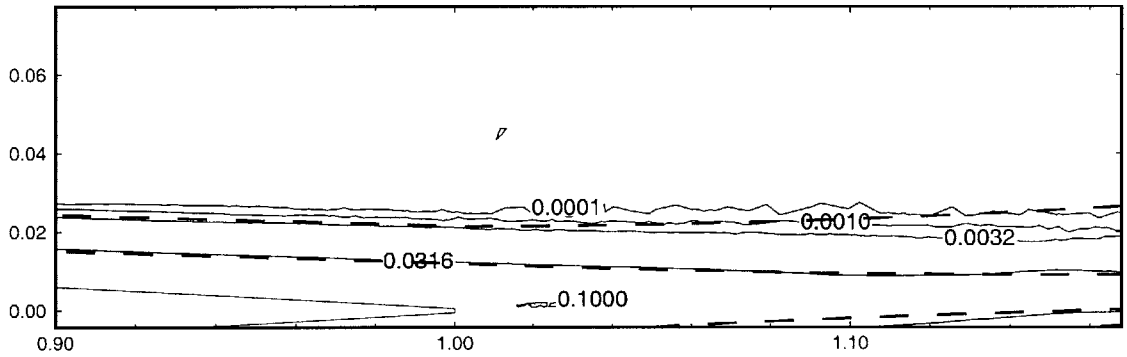

Figure 3-29: χ contours, trailing edge detail, $Re = 10^5$

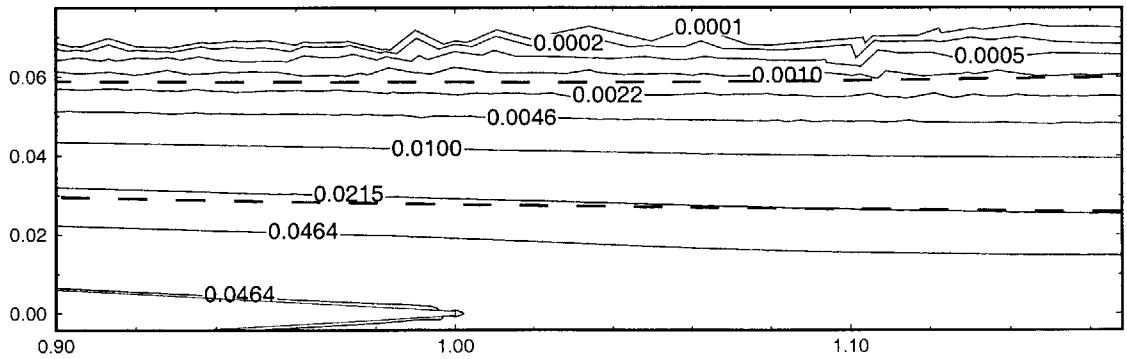

Figure 3-30: χ contours, trailing edge detail, $M = 0.2$

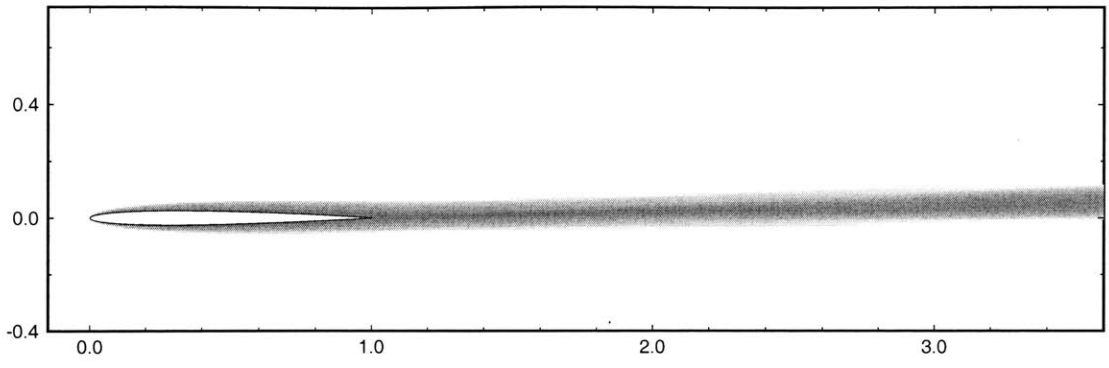

Figure 3-31: Shear layer visualization

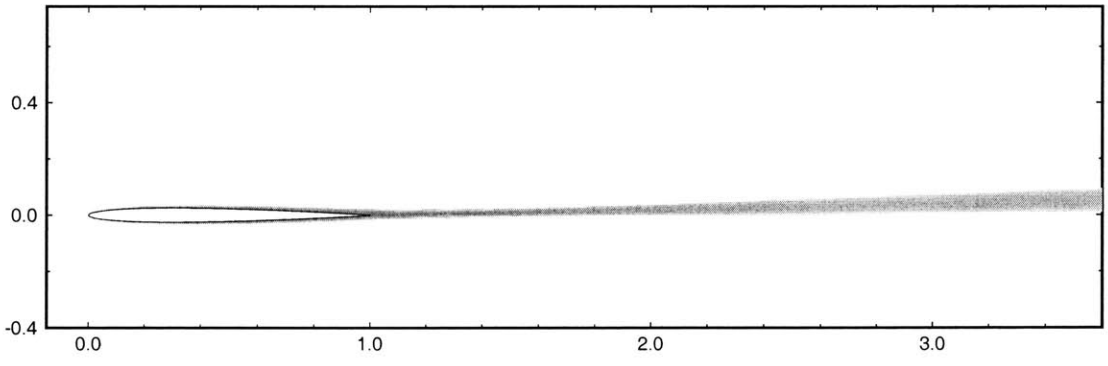

Figure 3-32: Visualization, $Re = 10^5$

3.2.3 Transonic RAE 2822 Airfoil

The first step in testing whether the shear layer detector rejects other flow features involves a flowfield with a normal shock. An RAE 2822 airfoil at flow conditions of $M = 0.73$, $Re = 6.5 \times 10^6$, and $\alpha = 1.5$ degrees carries a weak normal shock on its suction side (Figure 3-34). The shear layers in such a flow are for all practical purposes entirely turbulent. One aspect of the flow that we do wish the shear detector to pick up is the thickening of the boundary layer through the shock. To obtain a physically correct flow model, the solution from a FUN2D [1] simulation run by Venditti [26] was used as input to the shear detector equation, which was then run in a post-processing manner. The eddy viscosity information provided by FUN2D, summed with to the laminar viscosity, constitutes the viscosity used by the detector equation. The original solution contains no wake resolution, so the wake cannot be tracked in this test. Again an MSES simulation serves as the standard of comparison for the shear layer edge line. Velocity contours compare well with MSES (Figure 3-35).

The shear detector demonstrates excellent shock rejection. The rise in detector value behind the shock is slight, well below the shear layer edge threshold (Figure 3-36). The shock influences less finely-targeted properties such as entropy, as plotted in Figure 3-37. The detector also tracks boundary layer growth reasonably well through and downstream of the shock (Figure 3-39). Stability difficulties with the detector equation cropped up in the highly stretched cells in the boundary layer where oscillations are prone to blow up. Increased smoothing damps the oscillations effectively, although it also skews the detector solution slightly.

The velocity gradient tensor method again fared well (Figure 3-40). The fact that, in both methods, the detector contours wander across the boundary layer edge line slightly may mean that the detectors need to be calibrated to the turbulence model in question. This could be accomplished via additional diffusion and destruction terms in the style of equation 2.14. Some other physical effect may be at work, however, in which case an adjustment to the source term or some other remedy could be warranted. Figures 3-41 and 3-42 illustrate how the turbulent viscosity, governed in this case by the Spalart-Allmaras model [23], can serve as a conceptual basis for

a shear layer detector. Its contours follow the shear layer edge approximately as faithfully as our dedicated detector. In addressing the different and distinct goal of modeling turbulence, however, it falls to zero at the wall, which is not desirable for our purposes.

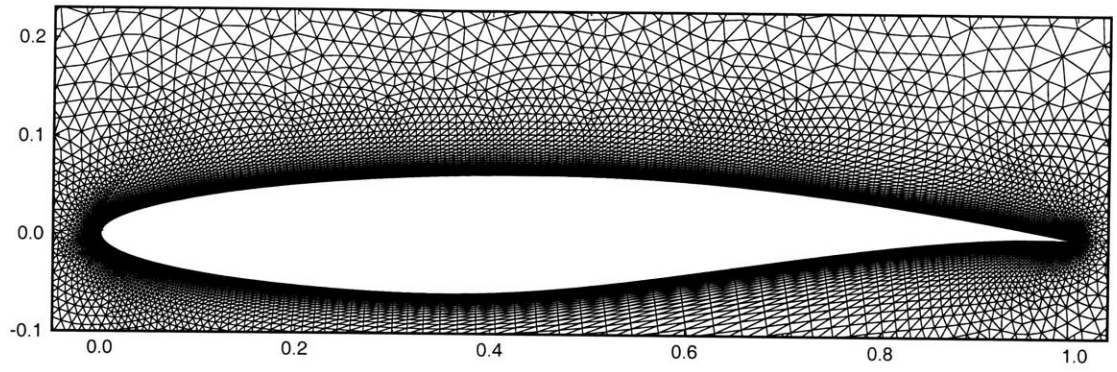

Figure 3-33: RAE 2822 computational grid

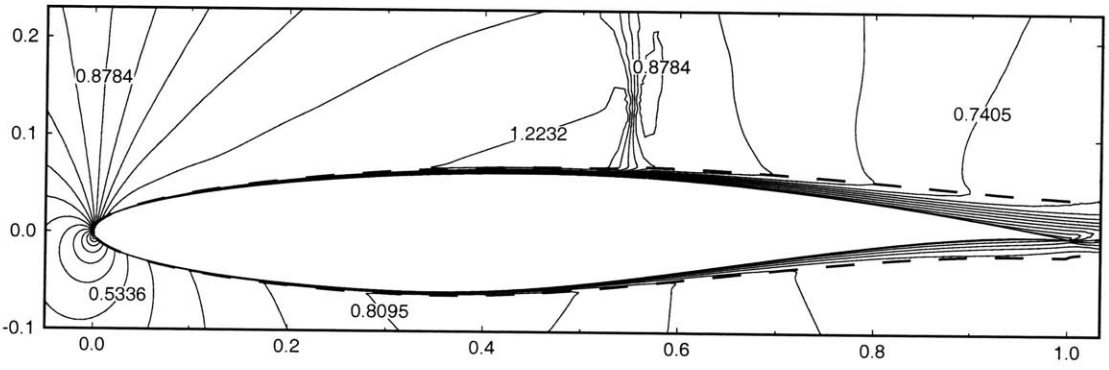

Figure 3-34: Mach contours

3.2.4 Multielement Airfoil

The laminar Navier-Stokes solver and shear detector were applied to a multielement high-lift airfoil, again with a grid created by Venditti [26]. This test purports to demonstrate the generality of the shear detection method to unsteady and separated

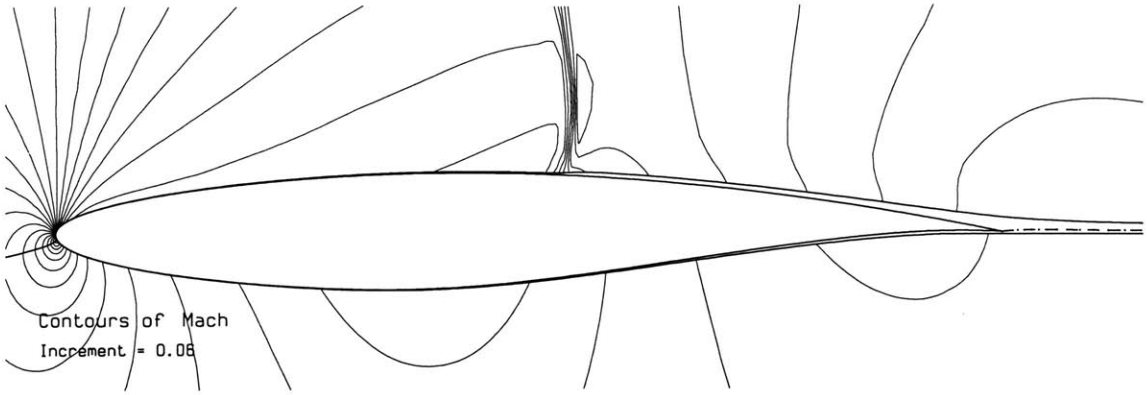

Figure 3-35: Mach contours using MSES

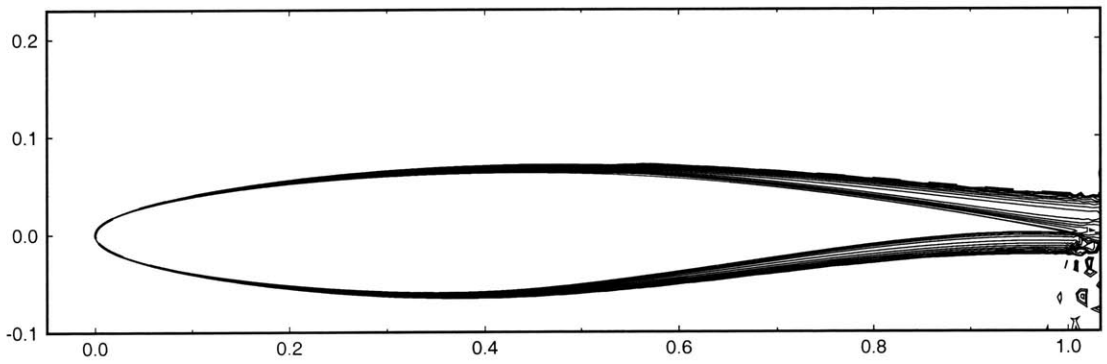

Figure 3-36: χ contours

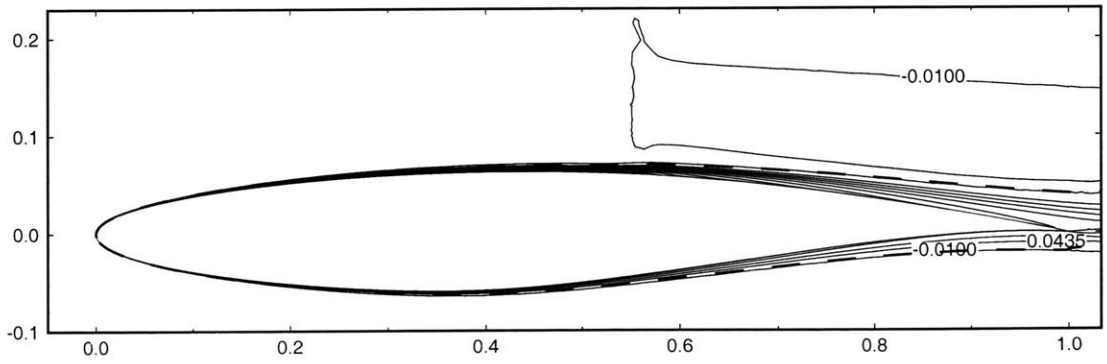

Figure 3-37: Entropy contours

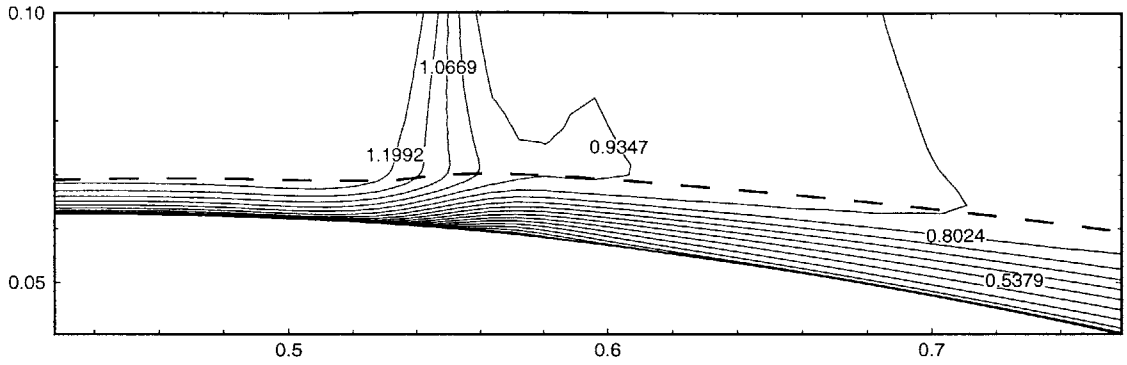

Figure 3-38: Mach contour shock detail, stretched y-axis

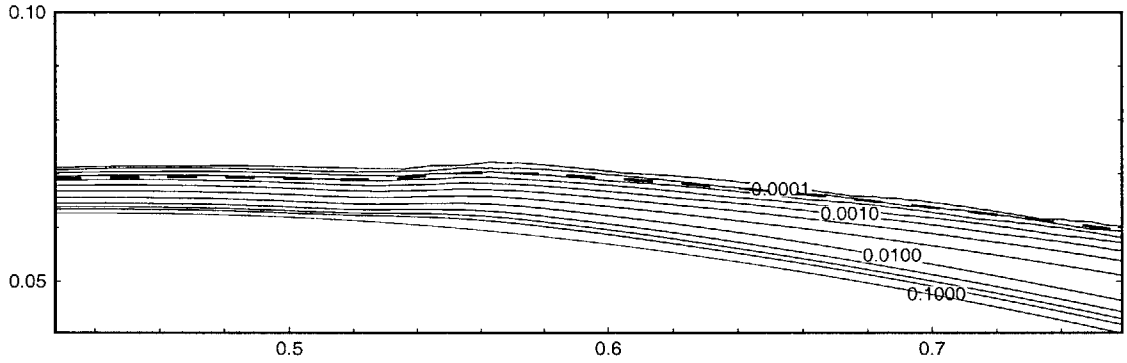

Figure 3-39: χ contour shock detail, stretched y-axis

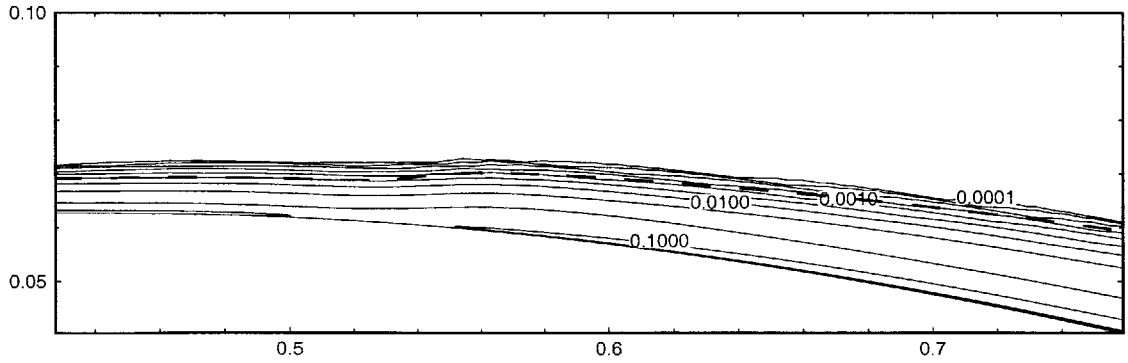

Figure 3-40: VGT χ contour shock detail, stretched y-axis

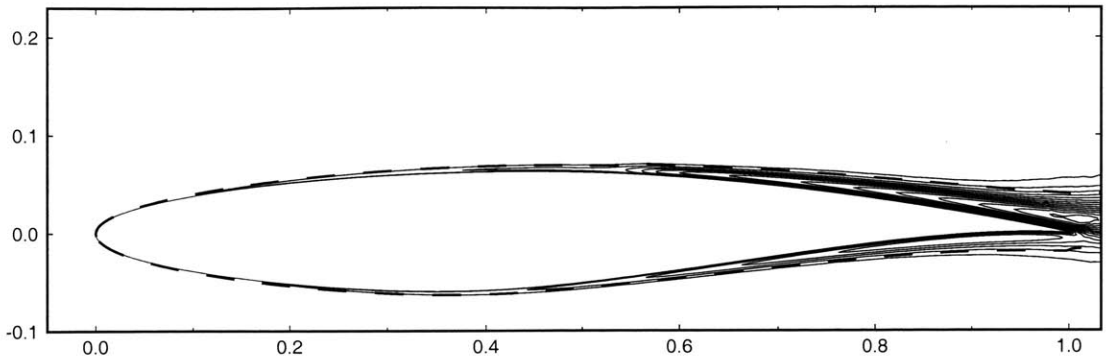

Figure 3-41: μ_t contours

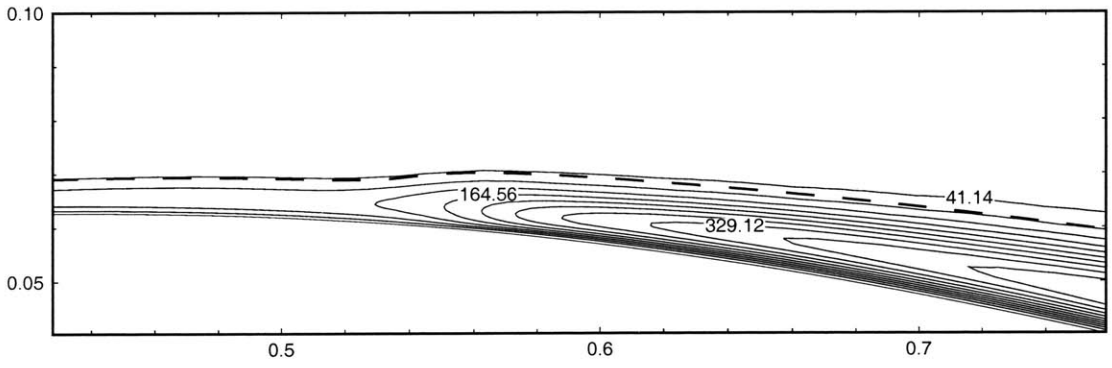

Figure 3-42: μ_t contour shock detail, stretched y-axis

flow. Farfield flow conditions are $Re = 1 \times 10^5$, $M = 0.2$, and $\alpha = 8.0$. Though the laminar modeling scheme is not truly accurate at these conditions and results in extensive flow separation, the experiment addresses not precision but generality.

Visualization of the shear detector shows that it tracks well with shear-influenced flow, most notably in the region between the first and second airfoil elements. The irregularity of the shear layer edge highlights how flow that is shed from the boundary layer mixes with the outer flow in an unsteady manner. The complexity of the computational geometry and the time dependence of the solution do not at all hinder the operation of the shear detector.

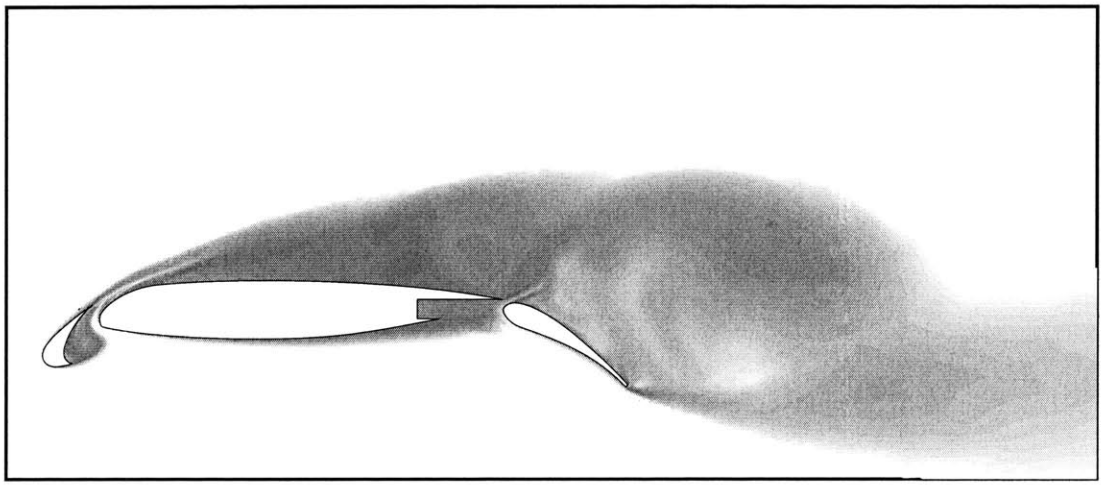

Figure 3-43: Three element airfoil shear layer visualization

Chapter 4

Three-Dimensional Approach

The last section validated the convective shear layer extraction technique for two-dimensional flows. To be a fully general feature extraction tool it must also perform well in three dimensions. Compared to flow simulations in two dimensions, three-dimensional flows present a great deal more difficulty in terms of constructing appropriate grids, modeling turbulence, and interpreting the resultant flowfield. As a consequence, the additional complexity of the third dimension makes shear layer extraction all the more attractive for solution improvement, visualization, and other purposes detailed in the Introduction. It is in unsteady three-dimensional simulations where feature extraction comes into its own as an essential interpretational tool.

The same shear layer extraction tactics as those used in two dimensions apply to three dimensions. A scalar detector variable, added to the state vector, time-marches with its own differential equation alongside the rest of the flow solution. An iso-surface of the detector variable at some threshold above zero denotes the outer bound of all shear regions in the flow.

4.1 Shear Detector Formulations

The shear detector equation itself, repeated here as Equation 4.1 for clarity, remains unchanged. The most significant modification from two dimensions is the construction of a three-dimensional source term.

$$\frac{\partial(\rho\chi)}{\partial t} + \nabla \cdot (\rho\chi\vec{q}) = \rho\Sigma \tag{4.1}$$

4.1.1 Navier-Stokes Equations Viscous Terms Source

In the three-dimensional Navier-Stokes momentum equations, the viscous terms from the equation for each Cartesian direction again form an element of a vector. Each vector component describes the local viscous deformation along its respective direction. The magnitude of the complete vector serves as an agglomerated description of the local amount of fluid shear. As before, μ includes the eddy viscosity in turbulent flows, and the Stokes hypothesis of $\lambda = -\frac{2}{3}\mu$ is expected to work well. The resultant shear detector scalar has units of velocity.

$$\nabla \cdot \bar{\bar{\tau}} = \begin{bmatrix} \frac{\partial}{\partial x}\left[2\mu\frac{\partial u}{\partial x} + \lambda\nabla\cdot\vec{q}\right] & + & \frac{\partial}{\partial y}\left[\mu\left(\frac{\partial u}{\partial y} + \frac{\partial v}{\partial x}\right)\right] & + & \frac{\partial}{\partial z}\left[\mu\left(\frac{\partial u}{\partial z} + \frac{\partial w}{\partial x}\right)\right] \\ \frac{\partial}{\partial x}\left[\mu\left(\frac{\partial v}{\partial x} + \frac{\partial u}{\partial y}\right)\right] & + & \frac{\partial}{\partial y}\left[2\mu\frac{\partial v}{\partial y} + \lambda\nabla\cdot\vec{q}\right] & + & \frac{\partial}{\partial z}\left[\mu\left(\frac{\partial v}{\partial z} + \frac{\partial w}{\partial y}\right)\right] \\ \frac{\partial}{\partial x}\left[\mu\left(\frac{\partial w}{\partial x} + \frac{\partial u}{\partial z}\right)\right] & + & \frac{\partial}{\partial y}\left[\mu\left(\frac{\partial w}{\partial y} + \frac{\partial v}{\partial z}\right)\right] & + & \frac{\partial}{\partial z}\left[2\mu\frac{\partial w}{\partial z} + \lambda\nabla\cdot\vec{q}\right] \end{bmatrix} \tag{4.2}$$

$$\rho\Sigma \equiv |\nabla \cdot \bar{\bar{\tau}}| \tag{4.3}$$

4.1.2 Velocity Gradient Tensor Quantities Source

The extension of the decomposed velocity gradient tensor source is less rudimentary than for the Navier-Stokes source. Batchelor [4] presents a pertinent discussion on relative motion near a point in a fluid. In the following discussion, the Cartesian construction description leads into the derivation of the more elegant generalized construction.

Cartesian Construction

An essential concept to recognize is that, on an elemental level, local fluid shear is a planar phenomenon. The decomposition diagrams from Section 2.1.2 can apply

equally well to planes within three-dimensional shearing flow. Vorticity and deformation out of the plane in question do not effect shearing flow considered within that plane. Taking a scalar measure of simple shear in each of three Cartesian planes generates three scalar terms, which can combine like a vector magnitude into a single all-encompassing scalar.

One approach is to charge ahead with an analogy to the Navier-Stokes viscous terms source. Each of the three momentum equations has scalar viscous terms that add to form an element of a vector, given in Equation 4.2. Similarly, the scalar measure of shear in each of the Cartesian planar directions can contribute an element to a vector description of local simple shear, the magnitude of which becomes the scalar source for the shear detector equation. The vorticity vector provides another relevant standard of comparison. Vorticity defined within each Cartesian plane has a direction perpendicular to that plane. The three components of vorticity combine to form a three-dimensional vector, the magnitude of which is the amount of local vorticity in the flow. In the same way, the three components of shear measure can constitute a vector description of the local shear. With respect to the task at hand, only the magnitude of the shear vector is important, but for other applications in which direction is significant, the vector form of local shear measure may prove useful.

As in the two-dimensional discussion, bulk expansion/contraction is removed from the velocity gradient tensor, and the velocity and deviatoric serve as building blocks for a simple shear element. Equation 4.7 makes apparent the assignment of deformation within a plane to the vector direction normal to that plane. The shear detector variable χ in the convection equation (4.1) has units of specific momentum.

$$\omega_{ij} = \left| \frac{\partial u_j}{\partial x_i} - \frac{\partial u_i}{\partial x_j} \right| \tag{4.4}$$

$$\bar{e}_{ij} = \sqrt{\left(\frac{\partial u_i}{\partial x_i} - \frac{\partial u_j}{\partial x_j} \right)^2 + \left(\frac{\partial u_i}{\partial x_j} + \frac{\partial u_j}{\partial x_i} \right)^2} \tag{4.5}$$

$$\Sigma_{ij} \equiv \nabla \left(\mu \sqrt{\omega_{ij} \bar{e}_{ij}} \right) \tag{4.6}$$

$$\vec{\Sigma} = \begin{bmatrix} \Sigma_{yz} \\ \Sigma_{zx} \\ \Sigma_{xy} \end{bmatrix} \tag{4.7}$$

$$\rho\Sigma = \rho\left|\vec{\Sigma}\right| \tag{4.8}$$

Generalized Construction

At any point in the flow at any given moment in time, vorticity can be represented as a single vector. At a point in space and time, rotation occurs around one axis at one rate: locally, vorticity is a planar phenomenon. Even though the deviatoric tensor is symmetric and can be broken down into a directional description, it does not readily reduce to a planar motion the way that vorticity does.

Equation 4.11 gives, in sequence, the bulk expansion/contraction, deviatoric, and vorticity matrices. The factor of $\frac{1}{3}$ in front of the bulk deformation matrix reflects the averaging of bulk deformation over three dimensions. The deviatoric matrix diagonal terms are in general nonzero, and although they are related to the off-axis terms through coordinate rotation, they are not simply interchangeable as in the two-dimensional case. Each diagonal entry contains information from all three dimensions, while the off-axis terms each contain information from only two dimensions.

$$\vec{q} = \begin{bmatrix} u \\ v \\ w \end{bmatrix} \tag{4.9}$$

$$\nabla\vec{q} = \begin{bmatrix} \frac{\partial u}{\partial x} & \frac{\partial u}{\partial y} & \frac{\partial u}{\partial z} \\ \frac{\partial v}{\partial x} & \frac{\partial v}{\partial y} & \frac{\partial v}{\partial z} \\ \frac{\partial w}{\partial x} & \frac{\partial w}{\partial y} & \frac{\partial w}{\partial z} \end{bmatrix} \tag{4.10}$$

$$\nabla\vec{q} = \frac{1}{3}\begin{bmatrix} \frac{\partial u}{\partial x}+\frac{\partial v}{\partial y}+\frac{\partial w}{\partial z} & 0 & 0 \\ 0 & \frac{\partial u}{\partial x}+\frac{\partial v}{\partial y}+\frac{\partial w}{\partial z} & 0 \\ 0 & 0 & \frac{\partial u}{\partial x}+\frac{\partial v}{\partial y}+\frac{\partial w}{\partial z} \end{bmatrix} \tag{4.11}$$
$$+ \frac{1}{2}\begin{bmatrix} \frac{2}{3}\left(2\frac{\partial u}{\partial x}-\frac{\partial v}{\partial y}-\frac{\partial w}{\partial z}\right) & \frac{\partial u}{\partial y}+\frac{\partial v}{\partial x} & \frac{\partial u}{\partial z}+\frac{\partial w}{\partial x} \\ \frac{\partial v}{\partial x}+\frac{\partial u}{\partial y} & \frac{2}{3}\left(2\frac{\partial v}{\partial y}-\frac{\partial w}{\partial z}-\frac{\partial u}{\partial x}\right) & \frac{\partial v}{\partial z}+\frac{\partial w}{\partial y} \\ \frac{\partial w}{\partial x}+\frac{\partial u}{\partial z} & \frac{\partial w}{\partial y}+\frac{\partial v}{\partial z} & \frac{2}{3}\left(2\frac{\partial w}{\partial z}-\frac{\partial u}{\partial x}-\frac{\partial v}{\partial y}\right) \end{bmatrix}$$
$$+ \frac{1}{2}\begin{bmatrix} 0 & \frac{\partial u}{\partial y}-\frac{\partial v}{\partial x} & \frac{\partial u}{\partial z}-\frac{\partial w}{\partial x} \\ \frac{\partial v}{\partial x}-\frac{\partial u}{\partial y} & 0 & \frac{\partial v}{\partial z}-\frac{\partial w}{\partial y} \\ \frac{\partial w}{\partial x}-\frac{\partial u}{\partial z} & \frac{\partial w}{\partial y}-\frac{\partial v}{\partial z} & 0 \end{bmatrix}$$

The most certain way to deal with divining directionalized shear information is to find the principal axes of the deviatoric. In the coordinate system defined by principal axes, the off-diagonal terms of the deviatoric vanish, and there may be a means of using the diagonal terms in the construction of a "deviatoric vector." A measure of local simple shear could then be constructed through a comparison of the vorticity vector (4.13) and the directional description of the deviatoric matrix. Such a comparison would assess whether vorticity and deviatoric strain operate in the same plane and at the same magnitude, which is the case when shearing flow is present.

$$\bar{\bar{\omega}} = \frac{1}{2}\begin{bmatrix} 0 & \frac{\partial u}{\partial y}-\frac{\partial v}{\partial x} & \frac{\partial u}{\partial z}-\frac{\partial w}{\partial x} \\ \frac{\partial v}{\partial x}-\frac{\partial u}{\partial y} & 0 & \frac{\partial v}{\partial z}-\frac{\partial w}{\partial y} \\ \frac{\partial w}{\partial x}-\frac{\partial u}{\partial z} & \frac{\partial w}{\partial y}-\frac{\partial v}{\partial z} & 0 \end{bmatrix} = \frac{1}{2}\begin{bmatrix} 0 & -\omega_z & \omega_y \\ \omega_z & 0 & -\omega_x \\ -\omega_y & \omega_x & 0 \end{bmatrix} \tag{4.12}$$

$$\vec{\omega} = \frac{1}{2}\begin{bmatrix} \omega_x \\ \omega_y \\ \omega_z \end{bmatrix} = \frac{1}{2}\begin{bmatrix} \frac{\partial w}{\partial y}-\frac{\partial v}{\partial z} \\ \frac{\partial u}{\partial z}-\frac{\partial w}{\partial x} \\ \frac{\partial v}{\partial x}-\frac{\partial u}{\partial y} \end{bmatrix} \tag{4.13}$$

The primary disadvantage of a principal axes-based generalized construction is that the process is computationally expensive. Finding the principal axes necessitates

the solution of a 3×3 matrix eigenvalue problem, which is costly to solve when applied to every point in the flow at every timestep. To reduce computational expense, there is a huge gain to be realized if there exists a way to take better advantage of the planar nature of shearing flow.

The desire to make use of a planar measure of local simple shear led to the main three-dimensional innovation presented in this thesis. As emphasized throughout this discussion, for two dimensions equal portions of vorticity and deviatoric strain are equivalent to simple shear. The vorticity acts in a plane (the "vortical plane"). The two-dimensional simple shear measure from Section 2.2 can apply to the deformation rate *in that plane.* Acknowledging that, as in two-dimensional analysis, it is gradients of simple shear that characterize a shear layer, the magnitude of the three-dimensional gradient of simple shear measure becomes the three-dimensional Σ. Deviatoric strain can take place outside of the vortical plane, but it contributes nothing to simple shear, so we need not consider it.

The vorticity magnitude $\omega = |\vec{\omega}|$ comes from its three-dimensional vector description (Equation 4.13). The deviatoric magnitude in the vortical plane, which requires a coordinate transformation, is given in Equation 4.14. In the primed coordinate system z' is aligned to the vorticity vector and x' and y' lie in the vortical plane with arbitrary orientation.

$$\bar{e}' = \sqrt{\left(\frac{\partial u'}{\partial x'} - \frac{\partial v'}{\partial y'}\right)^2 + \left(\frac{\partial u'}{\partial y'} + \frac{\partial v'}{\partial x'}\right)^2} \tag{4.14}$$

$$\rho\Sigma \equiv \rho \left| \nabla \left(\mu \sqrt{\omega \bar{e}'} \right) \right| \tag{4.15}$$

As in Equation 2.19, it is appropriate to include the viscosity when calculating Σ. Partial derivative values are more readily and cheaply obtained by evaluating them relative to the grid's coordinate system than relative to a local frame. Because it is a tensor, a rotation matrix T applied to the grid-frame velocity gradient tensor produces the correct tensor in the new rotated frame [24], as in Equation 4.16. The sequence for evaluating Σ at each node is therefore as follows:

1. Evaluate the velocity gradient tensor in the grid frame.

2. Use the velocity gradient tensor terms to find the vorticity vector $\vec{\omega}$.

3. Calculate the vorticity magnitude.

4. Find a rotation matrix that aligns the grid-frame z-axis to the vorticity vector.

5. Apply the rotation matrix to the velocity gradient tensor.

6. Use the rotated velocity gradient tensor terms to evaluate the planar deviatoric magnitude $\bar{e}'$.

7. Calculate the simple shear measure $\mu\sqrt{\omega\bar{e}'}$ at all nodes.

8. In the grid frame, take the magnitude of the simple shear gradient.

$$(\nabla\vec{q})' = T^T(\nabla\vec{q})T \tag{4.16}$$

The rotation matrix can be found in one of two ways. The first is to use the normalized vorticity vector as the third column of T and then, for the other two columns, find orthogonal unit vectors in the vortical plane. The second is to find the Euler angles between the grid-frame z-axis and $\vec{\omega}$ and use them to construct T. Note that only the first two Euler angles are necessary because the third involves rotation about the z-axis, which is arbitrary. In both cases the columns of T form the basis of the rotated frame.

The basic question is whether to consider the flow in three dimensions and then make a two-dimensional assessment of the degree of simple shear, as presented in the generalized method, or to consider the degree of shear in each Cartesian plane and, from that assessment, assemble a shear measure that is valid in three dimensions. Due to the planar nature of elemental shear, the generalized method is the clear choice because it addresses the problem directly and most likely with the greatest accuracy. Wherever boundary layer flow in a simulation becomes approximately two-dimensional, such as flow over a sailplane wing at a low angle of attack, the

generalized method explicitly reduces to the two-dimensional case regardless of the sailplane's orientation in the grid frame.

4.2 Verification

Implementation, as in two dimensions, consists of appending a shear detector variable to the state vector and iterating a convection equation alongside the flow equations, much like a one-equation turbulence model. Many three-dimensional viscous solvers are applicable to the task, among them the WIND code [5], which in its memory structure has accommodations for additional equations.

The options for validating the shear detection method for fully three-dimensional problems are limited. Though fundamentally a two-dimensional problem, it is useful to first validate the model on a flat plate test case, which then sets a standard for the edge threshold of the shear detector. From there validation can continue against the few analytical solutions available for three-dimensional boundary layer problems. Stagnation point flow, axially symmetric wake flow, and flow over a yawed cylinder are possibilities [21], although only the yawed cylinder problem is truly three-dimensional; the others are axially symmetric. IBLT models can also serve as standards for axially symmetric geometries. Should an iso-surface of the shear detector accurately match the shear layer edge surface for all attempted test cases, the detection method would be applicable to any arbitrary viscous flow geometry.

Chapter 5

Conclusions

5.1 Validity and Generality

To date, automated fluid feature extraction can reasonably address all features except for shear layers. Shear layers pose a particularly difficult problem because they are essentially undetectable in a local sense. If one desires to know whether a particular point in the flow is within a shear layer or not, information about the surrounding flow and the time history of the flow must be taken into account. The approach taken in this body of work bears a strong similarity to one-equation turbulence models, which represent turbulent flows via an eddy viscosity. Instead of modeling turbulent viscosity, in this investigation the measure in question is the degree to which shear has influenced the flow. A source term targets portions of the flow that exhibit high gradients of shear, and a convection equation uses that source to propagate the shear influence measure into the full extent of all shear layers present. A threshold of the shear detector scalar at a small increment above zero provides an iso-surface that matches the shear layers' edge. Both the Navier-Stokes equations viscous terms source and the velocity gradient tensor quantities source appear to be dependable, and the velocity gradient tensor source holds much promise for accurately singling out shearing flows in three dimensions, to the exclusion of other features.

Laminar flat plate, thin laminar airfoil, and transonic turbulent airfoil test cases demonstrate the validity of the convective shear layer feature extraction technique.

Validity is assured for laminar, incompressible flows in two dimensions. The technique also works well for compressible flows, aside from the fact that the threshold level exhibits some dependence upon Mach number. Given the threshold's good behavior with respect to Reynolds number, the possibility of similar performance with respect to Mach number is tantalizing. Though with the present formulation no one threshold value applies to all Mach numbers, the answer to the problem of a universal threshold value might lie in a different velocity gradient tensor quantities source or non-dimensionalization of the shear detector variable. For now the threshold for a particular Mach number comes from the flat plate test case.

As is intended, weak normal shocks are rejected as flow features. Although the technique is yet to be validated against curved shocks, supersonic flows, and three-dimensional vortical flows, its finely targeted source term should reject these flow features as well. One detail that approaches the philosophical is the issue of locating where the wake vanishes. In most CFD flows the "end of the wake" lies well beyond the domain, so this is not an issue. For far-wake studies or flows where wakes mingle with highly disturbed flow, such as rotor blade wakes on a helicopter, light application of dissipation and/or destruction terms in the convection equations may be appropriate to ensure that the detected wake eventually disappears into the surrounding flow.

The shear layer extraction tool is general to most flows of engineering interest. With the incorporation of the eddy viscosity and some adjustments specific to the turbulence model, turbulent shear flows can be found as well as laminar ones. There is no reason why the extraction method should not also function well in LES and DNS simulations. Fully developed internal flows may require special treatment, depending upon the application, to ensure that only the desired shear layers are detected as opposed to the entire flowfield. The technique is applicable on structured and unstructured grids, in two and three dimensions, and in both steady and unsteady simulations. It is in three-dimensional and unsteady flows that feature extraction tools become indispensable. Without them, the ability of CFD simulations to produce data outpaces the ability of human beings to fully interpret that data and sometimes even

outpaces the capability to store it at a reasonable cost. Shear layer feature extraction makes it practical for an investigator to assess the behavior of 3-D unsteady flow without probing at every point and at every timestep.

Computation can be executed either via post-processing or co-processing. Happily, the more empowering method of co-processing is actually computationally cheaper because the shear detector equation runs within the framework of the flow equations. Co-processing can make feature extraction an integral part of flow simulation and can enable a whole range of computational operations, from active solution improvement to great reductions in data writeout time and size. This investigation demonstrates the ready utility of active grid refinement in the wake, and other possibilities such as the use of the shear detector to drive improved algebraic turbulence models are yet to be explored.

5.2 Further Development

In the immediate future, the next steps for the shear extraction are implementation and test in three dimensions and spurious source rejection tests against all distinguishable types of flow features. The specific long-term implementation tool for our extraction tool is to incorporate it into the **F**luid Feature E**X**traction Tool-kit (FX) being developed by Haimes [15]. The FX package is capable of co- or post-processing three-dimensional flowfields using a variety of tools. Shear layer feature extraction, once mature, should become a widely-used component of CFD as it is applied to solution improvement, visualization, analysis, and design in fluid dynamics.

Bibliography

[1] W. Anderson and Daryl Bonhaus. An implicit upwind algorithm for computing turbulent flows on unstructured grids. *Computers and Fluids*, 23(1):1–21, 1994. http://fmad-www.larc.nasa.gov/~nielsen/Fun/fun.html.

[2] Barrett Baldwin and Harvard Lomax. Thin layer approximation and algebraic model for separated turbulent flows. In *AIAA 16th Aerospace Sciences Meeting*, Huntsville, Alabama, 16-18 January 1978. AIAA Paper 78-257.

[3] Lawrence Baskett and Robert Haimes. Feature extraction of shear layers. In *15th AIAA Computational Fluid Dynamics Conference*, Anaheim, California, 11-14 June 2001. AIAA Paper 2001-2665.

[4] G. K. Batchelor. *An Introduction to Fluid Dynamics*. Cambridge University Press, Cambridge, Great Britain, 1980.

[5] R. Bush, G. Power, and C. Towne. WIND: The production flow solver of the NPARC Alliance. In *36th Aerosciences Meeting & Exhibit*, pages 345–354, Reno, Nevada, 12-15 January 1998. AIAA Paper 98-0935. http://www.grc.nasa.gov/WWW/winddocs/.

[6] T. Cebeci and A. M. O. Smith. A finite-difference method for calculating compressible laminar and turbulent boundary layers. *Journal of Basic Engineering*, 92(3):523–535, September 1970.

[7] Mark Drela and Michael Giles. Viscous-inviscid analysis of transonic and

low Reynolds number airfoils. *AIAA Journal*, 25(10):1347–1355, 1987. http://raphael.mit.edu/projects%26research.html.

[8] Mark Drela, Ali Merchant, and Jaime Peraire. Elimination of spurious loss in Euler equation computations. In *29th AIAA Fluid Dynamics Conference*, Albuquerque, New Mexico, 15-18 June 1998. AIAA Paper 99-2424.

[9] NASA Dryden Flight Research Center Photo Gallery. http://www.dfrc.nasa .gov/gallery/photo/index.html.

[10] Robert W. Fox and Alan T. McDonald. *Introduction to Fluid Mechanics*. John Wiley & Sons, Inc., New York, fourth edition, 1992.

[11] Robert Haimes. Automated feature extraction from transient CFD simulations. In *Proceeding of the 7th Annual Conference of the CFD Society of Canada*, Halifax, Nova Scotia, May 1999. Keynote address.

[12] Robert Haimes. Using residence time for the extraction of recirculation regions. In *A Collection of the 14th AIAA Computational Fluid Dynamics Conference Technical Papers*, volume 1, pages 345–354, Norfolk, Virginia, 28 June-1 July 1999. AIAA Paper 99-3291.

[13] Robert Haimes and Kirk Jordan. A tractable approach to understanding results from large-scale 3D transient simulations, January 2001. AIAA Paper 2001-0918.

[14] Robert Haimes and David Kenwright. On the velocity gradient tensor and fluid feature extraction. In *A Collection of the 14th AIAA Computational Fluid Dynamics Conference Technical Papers*, volume 1, pages 315–324, Norfolk, Virginia, 28 June-1 July 1999. AIAA Paper 99-3288.

[15] Robert Haimes and David Kenwright. *FX Programmer's Guide*. Massachusetts Institute of Technology, 0.90 (beta) edition, 10 July 2000. The **F**luid Feature E**X**traction Tool-Kit. http://raphael.mit.edu/fx/.

[16] A. Jameson. Numerical solution of the Euler equations by finite volume methods using Runge-Kutta time stepping schemes, 1981. AIAA Paper 81-1259.

[17] David Kenwright. Automatic detection of open and closed separation and attachment lines, 1999. AIAA Paper.

[18] Langley Image Scanning, Archival, and Retreival. NASA Langley Research Center. http://lisar.larc.nasa.gov/LISAR/.

[19] David Lovely. Boundary layer and shock detection in CFD solutions. Master's thesis, Massachusetts Institute of Technology, Department of Aeronautics and Astronautics, February 2000.

[20] Ali Merchant. Personal communication.

[21] Hermann Schlichting. *Boundary-Layer Theory.* McGraw-Hill Book Company, New York, seventh edition, 1979.

[22] Jonathan Shewchuk. Triangle: Engineering a 2D quality mesh generator and Delaunay triangulator. In *First Workshop on Applied Computational Geometry*, pages 124–133. ACM, May 1996. http://www-2.cs.cmu.edu/~quake/triangle.html.

[23] P. R. Spalart and S. R. Allmaras. A one-equation turbulence model for aerodynamic flows. In *30th Aerospace Sciences Meeting & Exhibit*, Reno, Nevada, 6-9 January 1992. AIAA Paper 92-0439.

[24] Gilbert Strang. *Introduction to Applied Mathematics.* Wellesley-Cambridge Press, Wellesley, Massachusetts, 1986.

[25] Milton Van Dyke. *An Album of Fluid Motion.* The Parabolic Press, Stanford, California, 1998.

[26] David Venditti. Personal communication.

[27] Frank M. White. *Viscous Fluid Flow.* McGraw-Hill, Boston, second edition, 1991.

[28] http://aerodyn.org/Miscellanea/quotes.html.

3231-10